On models of double porosity poroelastic media

Claude Boutin, Pascale Royer

On models of double porosity poroelastic media

Claude Boutin[1] and Pascale Royer[2]

[1] *Université de Lyon - Ecole Nationale des Travaux Publics de l'Etat - LGCB - CNRS 5513 F-69518 Vaulx-en-Velin, France. E-mail: claude.boutin@entpe.fr*
[2] *Laboratoire de Mécanique et Génie Civil (LMGC), UMR 5508 CNRS, Université de Montpellier, F-34095 Montpellier Cedex 5, France*

SUMMARY

This paper focuses on the modelling of fluid-filled poroelastic double porosity media under quasi-static and dynamic regimes. The double porosity model is derived from a two-scale homogenization procedure, by considering a medium locally characterized by blocks of poroelastic Biot microporous matrix and a surrounding system of fluid-filled macropores or fractures. The derived double porosity description is a two-pressure field poroelastic model with memory and viscoelastic effects. These effects result from the 'time-dependent' interaction between the pressure fields in the two pore networks. It is shown that this homogenized double porosity behaviour arises when the characteristic time of consolidation in the microporous domain is of the same order of magnitude as the macroscopic characteristic time of transient regime. Conversely, single porosity behaviours occur when both timescales are clearly distinct. Moreover, it is established that the phenomenological approaches that postulate the coexistence of two pressure fields in 'instantaneous' interaction only describe media with two pore networks separated by an interface flow barrier. Hence, they fail at predicting and reproducing the behaviour of usual double porosity media. Finally, the results are illustrated for the case of stratified media.

Key words: Geomechanics; Microstructures; Permeability and porosity; Elasticity and anelasticity; Wave propagation; Mechanics, theory, and modelling.

1 INTRODUCTION

The fluid–solid coupling effects in porous geological formations are key phenomena in various fields of applications of earth sciences. These include oil, groundwater, environmental, geothermal, geotechnical, geophysical engineering, where a clear understanding of the physical mechanisms governing fluid flows, heat and mass transfer, consolidation and wave propagation are very important. For instance, the knowledge of seismic wave attenuation and dispersion resulting from wave-induced flow in porous rocks (see the review Müller *et al.* 2010) is crucial in petroleum engineering or in hydrogeology (e.g. Pride 2005) to assess reservoir properties such as porosity and permeability from the inversion of geophysical data. In oil extraction or CO_2 storage, a decrease or increase in pore pressure may result either in a sudden induced seismicity, or a slow phenomenon of subsidence or inverse subsidence. At larger scale, similar phenomena are reported in seismology, where the pore pressure diffusion appears to be a triggering mechanism of some earthquake swarm (Parotidis *et al.* 2003). In these examples, the records of micro tremors, micro seismic data or the monitoring of non steady state phenomena are used to extract physical properties of porous rocks by inversion (Shapiro 2000). Thus, the relevancy of geotomography imaging by down-scaling strongly depends on the poroelastic model used in the inversion procedure. The reference model established by Biot (1956a,b) is perfectly appropriate for geological formation that present a quasi-uniform pore distribution, that is, a single porosity structure. However, geological porous formations often exhibit a variety of heterogeneities such as fractures, fissures, cracks and macropores or interaggregate. The double porosity of these media is a consequence of either the geological processes themselves or from industrial fracturing which aims at recovering more efficiently oil, hot water, or gas. Thus, the existence of accurate models for predicting double porosity effects is of particular practical interest, see for example Brajanovski *et al.* (2006), Grechka *et al.* (2010). Double porosity modelling has thus become the subject of vast research since the introduction of the concept and first models Barenblatt *et al.* (1960), Barenblatt (1963).

The focus of the present study is on the fundamentals of poroelastic double porosity media, that is, fluid-filled elastic media that consist of two interacting porous systems of significantly different permeabilities: a microporous matrix continuum of low permeability and a fracture or macropore continuum of high permeability. Biot's theory (Biot 1956a,b) which describes single porosity poroelastic media (Auriault & Sanchez-Palencia 1977), (Auriault 1980), generally fails in reproducing the behaviour of double porosity media. This is due to the permeability

contrast which induces different pressure fields in the micropores and macropores. This generally results in two pressure fields that interact at the macroscale and, therefore, in an enriched Biot description.

Among the significant amount of literature devoted to double porosity modelling, two main approaches to modelling double porosity media may be distinguished, that is, phenomenological and upscaling approaches. The former ones are based on postulating the model directly on macroscopic scale, while in upscaling approaches the macroscopic model is deduced from the governing equation at the local scale. Phenomenological modelling of double porosity media was initiated in Barenblatt *et al.* (1960), Barenblatt (1963) using the theory of mixtures for modelling fluid flow in rigid fractured porous media. This model was further modified by Warren & Root (1963) to account for permeability contrast. In these models, the coexistence of two pressure fields in linear *instantaneous* interaction is directly postulated on the macroscopic scale. These models were then extended to poroelastic double porosity media by combining Biot's theory with either Barenblatt or Warren and Root models (Wilson & Aifantis 1982; Beskos & Aifantis 1986; Bai *et al.* 1993; Berryman & Wang 1995). In all of them, the influence of the microstructure on the macroscopic behaviour is postulated via the coupling term between both pressure fields. Their validity is thus conjectured, but not rigorously proven.

Regarding upscaling approaches, the homogenization method of multiscale asymptotic expansions (Sanchez-Palencia 1980) allows to explicitly linking the microstructural behaviour with the macroscopic description. The first results related to double porosity using the homogenization method are those developed in Auriault (1983), and then in Arbogast (1989) and Arbogast *et al.* (1990), where two-scale upscaling was performed on rigid media presenting a high contrast in thermal conductivities or permeabilities, respectively. In Auriault & Boutin (1992) and Auriault & Boutin (1993), the deformation of the skeleton is accounted for by considering an elastic hierarchical porous structure. A three-scale medium with three separate scales was considered. These scales were the microscale (associated to the micropores), the mesoscale (related to the macropores or fractures) and the macroscale which is the scale of the global phenomenon. Instead of a hierarchical morphology, a medium locally characterized by blocks of poroelastic Biot microporous matrix and a surrounding system of fluid-filled macropores is considered in Murad *et al.* (2001), where a two-scale homogenization procedure together with a two-level finite element approach was applied. The common result of these works on double porosity poroelastic media is a model with two pressure fields 'in time-dependent interaction' obtained when the microscale/mesoscale ratio is of the same order of magnitude as the meso/macro scale ratio. This two-pressure field model suggests that the micropore pressure is inhomogeneous while the macropore pressure is homogeneous. Due to the fluid–solid interaction the inhomogeneity of the micropore pressure gives rise to an apparent macroscopic viscoelastic behaviour of the microporous matrix. This double porosity model reduces to single porosity Biot models when the micro/meso and the meso/macro scale ratios are of distinct orders of magnitude. Two single-porosity models are thus obtained, which are distinguished by their effective elastic properties, and depend on whether the micro/meso scale ratio is smaller or larger than the meso/macro one (Auriault & Boutin 1992, 1993). Note that these rules in terms of the respective orders of magnitude of the scale ratios can easily be expressed as orders of magnitude of the permeability contrast between the micropores and the macropores. The above analysis highlights the key role of the permeability contrast in double porosity modelling. Similar homogenization approaches have then been applied to study poroelastic dynamics (see for example in Auriault & Boutin 1994; Pride & Berryman 2003, where the volume-averaging method was used), highly compressible fluid flow (Royer & Auriault 1994), acoustics of air saturated rigid porous media (Boutin *et al.* 1998; Venegas & Umnova 2011), and solute transfer in porous media (Auriault & Lewandowska 1995). In the latter two contexts the theory has been experimentally validated (Olny 1999; Olny & Boutin 2003; Ngoc *et al.* 2007; Lewandowska *et al.* 2008).

The aim of the present paper is to analyse the above cited homogenized poroelastic double porosity models, paying particular attention on their effective parameters properties and on the interpretation of their domains of validity. To do so, the three following main points are addressed:

(1) The study carried out in (Auriault & Boutin 1992, 1993) is revisited using a two-scale instead of a three-scale homogenization procedure. As shown in the original works, the micro/meso upscaling leads to a Biot model for the microporous medium on the mesoscopic scale. Hence, the study can be reduced to a two-scale approach by considering the meso/macro upscaling of a heterogeneous medium made of connected macropores (or fissures) surrounded by a Biot material. This two-scale homogenization formulation significantly simplifies the derivation of the macroscale model, the identification of the key dimensionless parameters and the determination of the symmetry properties of the description.

(2) The physical meaning of the models' domains of validity is analysed. As shown in Royer & Boutin (2012) for fluid flow and solute transport in rigid double porosity media, the model's domains of validity—which from the raw results of the homogenization procedure arise as a function of the magnitude of the length-scale ratio (or permeability contrast)—can be expressed as a function of the magnitude of the timescale ratio. It is thus shown that a given double porosity medium may either behave as a single or as a double porosity one according to the considered timescale. Single porosity behaviours occur at short term (only the macropore porosity is accounted for) or at long term (the total porosity of the double porosity medium is taken into account), while double porosity behaviour arises whenever the timescale of the global phenomenon is of the same magnitude as the timescale of the local phenomenon in the microporous domain.

(3) The validity of the usual phenomenological double porosity models is commented in light of the results provided by homogenization theory. It is worth mentioning that it has already been pointed out that homogenized and phenomenological models do not match or only partially match (Hornung & Showalter 1990; Auriault & Royer 1993; Royer & Auriault 1994). This issue is tackled by showing that double porosity phenomenological models correspond to homogenized models obtained for media made of two distinct permeable domains separated by an interface flow barrier.

The paper is organized as follows. In Section 2, we briefly introduce the principles of the homogenization method. Then, Section 3 is devoted to the formulation and the analysis of the physics at the local scale. The macroscopic description is derived and presented in Section 4. Since the focus is put on the influence of double porosity microstructure, these developments are performed in quasi-static regime. Section 5 deals with a time analysis used to determine the domains of validity of the models while Section 6 aims at comparing homogenized and phenomenological models. An example of a stratified medium is considered in Section 7. Finally, Section 8 is devoted to the extension of the results to dynamic regime and gives a simple numerical illustration of the theory. The calculations details related to the homogenization procedure and to the properties of the effective parameters are reported in Appendices A and B.

2 PRINCIPLES OF THE HOMOGENIZATION METHOD

The aim of homogenization techniques is to model an heterogeneous medium as an equivalent continuous medium, whose description is valid at a very large scale compared to that of the heterogeneities. The homogenization of a medium with a high density of heterogeneities is only possible if we consider regions containing a large number of them. In other words, the continuum macroscopic representation of an heterogeneous medium makes sense only when a separation of length scales exists. This implies that Auriault (1991), Auriault *et al.* (2009); (i) the material is regular enough so that a representative elementary volume (REV) of characteristic size l can be identified at the heterogeneity scale. This will be referred to as the microscopic, or local scale, as opposed to the macroscopic scale, which is the scale the equivalent continuum is defined at; (ii) the physical variables driving the phenomenon vary according to the macroscopic size L, which is much greater than l.

With the asymptotic two-scale homogenization method (Sanchez-Palencia 1980), the above requirements are mathematically expressed as follows. First, the medium is assumed to be periodic and made of identical cells $\widehat{\Omega}$ of size ℓ. Thus, the REV is simply the periodic cell. Note that the periodicity assumption is not a restriction when looking for the structure of the macroscopic description and the properties of the effective parameters, since non-periodic and periodic media are equivalent when homogenization is possible, which occurs when the length scales are separated (Auriault *et al.* 2009). Second, two space variables are defined to describe the variations on both distinct length scales L and ℓ: $\mathbf{x}$ for the macroscopic variations, $\mathbf{y}$ for the microscopic variations. The key parameter of the method is the scale ratio defined as

$$\varepsilon = l/L \ll 1, \tag{2.1}$$

The space variables are linked by

$$\mathbf{y} = \varepsilon^{-1}\mathbf{x}, \tag{2.2}$$

and are from now on treated as two independent space variables. Finally, the unknown fields (e.g. pressure p, solid motion $\underline{u}$ and so on) are looked for in the form of asymptotic expansions in powers of ε and are $\widehat{\Omega}$-periodic in variable $\mathbf{y}$, as a result of material periodicity and length-scale separation:

$$p(\mathbf{x},\mathbf{y}) = \sum_0^\infty \varepsilon^i p^i(\mathbf{x},\mathbf{y}) \qquad \text{with} \qquad p^i(\mathbf{x},\mathbf{y}) \quad \widehat{\Omega}-\text{periodic in } \mathbf{y}. \tag{2.3}$$

The method consists in expressing the local governing equations into a dimensionless form, which gives rise to dimensionless parameters. The orders of magnitude of these dimensionless parameters are estimated in power of the scale ratio ε. Introducing these estimates into the two-scale set of partial differential equations—where the spatial derivative ∂ reads $\varepsilon^{-1}\partial_y + \partial_x$—provides the rescaled equations on which the homogenization process is performed. Identifying the terms of the same power in ε, and solving the boundary value problems obtained in series yield the first non-trivial balance equation. This defines the homogenized model and effective parameters valid up to the leading order. Energetic consistency between micro and macro descriptions is ensured by the method itself.

3 LOCAL DESCRIPTION OF POROELASTIC DOUBLE POROSITY MEDIUM

3.1 Problem statement

We investigate the behaviour of a fluid-saturated deformable elastic double porosity media (see examples on Fig. 1). The local structure is periodic with period $\widehat{\Omega} = \Omega \cup \Omega_p$ (which is therefore the representative elementary volume REV). Here Ω is the fluid-saturated microporous domain, Ω_p is the pore space occupied by the fluid and $\Gamma = \partial\Omega \cap \partial\Omega_p$ represents the surface of the microporous matrix. The same fluid occupies both the microporous domain and the pore space. We denote by ℓ and L the characteristic size of the period (i.e. the microscopic size) and the macroscopic characteristic size, respectively. The porosity of the microporous domain is denoted by ϕ, while the pore porosity is defined as $\phi_p = |\Omega_p|/|\widehat{\Omega}|$. Consequently, the total medium porosity is given by: $\Phi = \phi_p + (1-\phi_p)\phi$. We investigate the behaviour of the medium when subjected to a harmonic regime of frequency $f = \omega/2\pi$. Note that the time-dependent term $e^{i\omega t}$ is omitted in all the equations because of the linearity of the problem. Since our objective is to focus on double porosity effects, the detailed developments are performed in a quasi-static regime, that is, for a frequency which is sufficiently low so that inertial effects are negligible on the macroscale. The double porosity features of the behaviour are thus clearly highlighted. Extension to the derivation of the model in dynamic regime is straightforward, as it will be shown in Section 8.

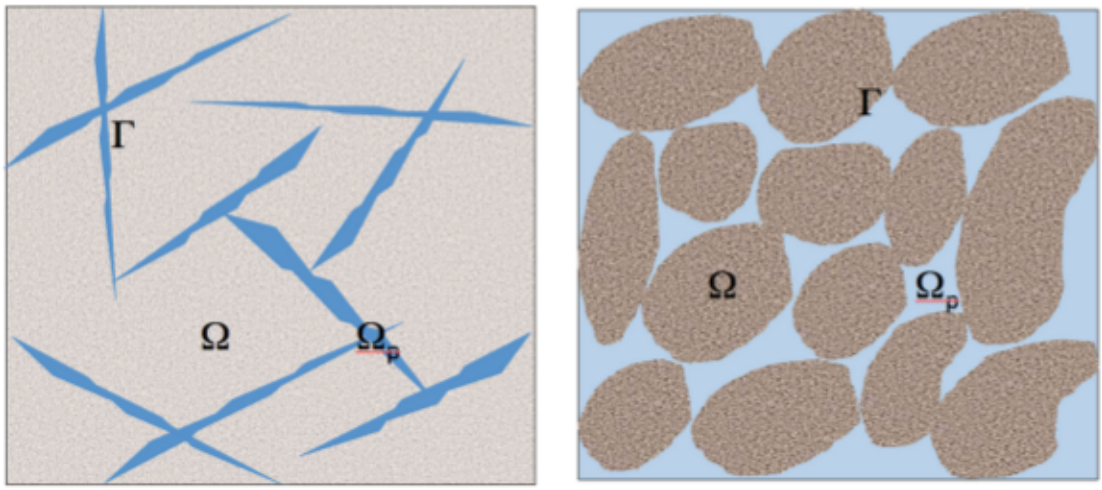

Figure 1. Examples of morphologies of double porosity media considered by homogenization. Left: fissured microporous material, Right: microporous medium with pore network.

3.2 Governing equations in the microporous domain Ω

We consider that the microporous matrix is a poroelastic medium which satisfies the classical Biot single porosity model (Biot 1956a,b; Auriault 1980): The governing equations are the following ($\dot{}$ stands for time derivative):

$$\left.\begin{aligned} \underline{\mathrm{div}}(\boldsymbol{\Sigma}) &= \underline{0} \\ \boldsymbol{\Sigma} &= \mathbf{c} : \mathbf{e}(\underline{u}) - \boldsymbol{\alpha} p \\ \mathrm{div}(\underline{q}) &= -\boldsymbol{\alpha} : \mathbf{e}(\dot{\underline{u}}) - \frac{\dot{p}}{M} \\ \underline{q} = \phi(\underline{v}_f - \dot{\underline{u}}) &= -\frac{\mathbf{K}}{\eta}.\underline{\mathrm{grad}}(p) \end{aligned}\right\} \tag{3.1}$$

These four equations express the momentum balance (3.1–a), the poroelastic constitutive law (3.1–b), the conservation of fluid mass (3.1–c) and Darcy's law (3.1–d), respectively. The distinct quantities involved in the model are defined as follows:

(i) $\boldsymbol{\alpha}$ represents the symmetric and positive Biot coupling tensor. For isotropic microporous matrix, $\boldsymbol{\alpha} = \alpha \mathbf{I}$, where $\alpha = 1 - K/K_s$ is Biot's coefficient, and K and K_s represent the bulk moduli of the empty (or drained) microporous matrix and of the elastic material forming the microporous matrix, respectively. Note further that: $\phi \leq \alpha \leq 1$;

(ii) $1/M$ is Biot's bulk modulus: $\frac{1}{M} = \frac{\alpha - \phi}{K_s} + \frac{\phi}{K_f}$, where K_f is the fluid bulk modulus;

(iii) $\mathbf{c}$ is the effective elastic tensor of the empty (i.e. dry or 'drained') microporous skeleton. As an elastic tensor, it satisfies: (1) the ellipticity condition ($\exists a > 0 \,/\, \forall \mathbf{e}\,;\, \mathbf{e}:\mathbf{c}:\mathbf{e} \geq a\, \mathbf{e}:\mathbf{e}$); (2) minor symmetry($c_{ijkl} = c_{jikl} = c_{ijlk}$) and (3) major symmetry ($c_{ijkl} = c_{klij}$). For an isotropic matrix, it reduces to the Lamé coefficients λ and μ. The bulk modulus of the empty matrix K, and the Poisson ratio ν are denoted $K = \lambda + 2\mu/3$, $\nu = \lambda/2(\lambda + \mu)$, respectively. In what follows, we will also make use of the 'consolidation' bulk modulus B, defined as $\frac{1}{B} = \frac{1}{M} + \frac{\alpha^2}{\lambda + 2\mu}$, and of the short-term (or 'undrained') parameters $\lambda_\infty = \lambda + \alpha^2 M$, $K_\infty = \lambda_\infty + 2\mu/3$ and $\nu_\infty = \lambda_\infty/2(\lambda_\infty + \mu)$;

(iv) $\underline{u}$ is the solid displacement of the microporous matrix, while $\underline{v}_f$ stands for the mean fluid velocity within the volume of the micropores. In harmonic regime, it is convenient to introduce the mean fluid motion: $i\omega \underline{u}_f = \underline{v}_f$. Darcy's flux is thus given by: $\underline{q} = \phi(\underline{v}_f - \dot{\underline{u}}) = i\omega\phi(\underline{u}_f - \underline{u})$;

(v) $\mathbf{e}(\underline{u})$ is the strain tensor, while $\boldsymbol{\Sigma}$, $\boldsymbol{\sigma} = \mathbf{c} : \mathbf{e}(\underline{u})$ and p represent the tensor of total stress, the tensor of effective stress (i.e. the mean stress in the solid skeleton), and the interstitial pressure, respectively;

(vi) η is the fluid viscosity and $\mathbf{K}$ the tensor of intrinsic permeability, which for an isotropic microporous matrix is such that $\mathbf{K} = K\mathbf{I}$.

3.3 Governing equations of the fluid in the pore domain Ω_p

In the pore domain Ω_p, the fluid motion is governed by the following linear differential set of equations:

$$\left.\begin{aligned} \underline{\mathrm{div}}(\boldsymbol{\sigma}_p) &= \underline{0} \\ \boldsymbol{\sigma}_p &= -p_p \mathbf{I} + 2\eta \mathbf{D}(\underline{v}_p) \\ \mathrm{div}(\underline{v}_p) &= -\frac{\dot{p}_p}{K_f} \end{aligned}\right\} \tag{3.2}$$

These equations express the momentum balance (3.2–a), the viscous constitutive law (3.2–b) and the conservation of fluid mass (3.2–c), respectively. Note that all fields in the pore domain Ω_p are indexed by $_p$. In the above equations, $\boldsymbol{\sigma}_p$ and p_p stand for the stress tensor and the pressure of the fluid, respectively; $\underline{v}_p = i\omega\underline{u}_p$ represents the fluid velocity and $\underline{u}_p$ is the fluid displacement; $\mathbf{D}(\underline{v}_p) = i\omega\mathbf{e}(\underline{u}_p)$ is the strain rate tensor.

3.4 Boundary conditions over the interface Γ between microporous matrix and pore domain

Over the interface, we express the continuity of normal stresses (3.3–a), of pressures(3.3–b), and of the fluid mass fluxes (3.3–c) as:

$$\left.\begin{aligned} \boldsymbol{\Sigma}.\underline{n} = \boldsymbol{\sigma}_p.\underline{n} \\ p = p_p \\ \underline{q}.\underline{n} = \phi(\underline{v}_f - \dot{\underline{u}}).\underline{n} = (\underline{v}_p - \dot{\underline{u}}).\underline{n} = \underline{q}_p.\underline{n} \end{aligned}\right\} \tag{3.3}$$

3.5 Order and scale estimates

From former studies (Auriault & Boutin 1992, 1993), it is known that the above local description gives rise to three homogenized models: a double porosity model and two distinct single porosity models. But as particularly emphasized in the review (Royer & Boutin 2012), the double porosity model is more general, since it can reduce to either of the single porosity models. Mathematically, this reduction consists in a simple continuous passage and corresponds to the order of magnitude variations of the key physical parameters. Here, our objective is to *a priori* identify, by means of physical arguments, the conditions under which a double porosity macroscopic model is obtained.

To describe non stationary regimes at the macroscale we determine the macroscopic characteristic time first. From single porosity studies, it is known that this corresponds to a consolidation process characterized by fluid flow and solid deformation mechanisms of comparable importance. More precisely, this occurs whenever the rate of volume variation

$$\mathrm{div}(\dot{\underline{u}}) = O(\dot{p}_p/|B|),$$

with

$$O(|B|^{-1}) = O(M^{-1} + |\mathbf{c}|^{-1}),$$

in which B accounts for both fluid and solid moduli, is balanced by the Darcy's flow

$$\mathrm{div}(\underline{q}_p) = (\mathrm{K}_p/\eta)\mathrm{div}(\underline{\mathrm{grad}}(p_p)) = O(\mathrm{K}_p/\eta)O(p_p/L^2).$$

Hence, in transient regime, the macroscopic characteristic time T (of associated angular frequency $\omega = 2\pi/T$) is linked to the macroscopic length L by the following relationship:

$$T = O\left(2\pi\frac{\eta}{|B|}\frac{L^2}{\mathrm{K}_p}\right) \tag{3.4}$$

Let us now focus on the permeability contrast, which is a key parameter since it determines the fluid flow interactions between both porous networks. Indeed, an extremely high contrast entails an apparent quasi-impervious microporous matrix. As a result, the fluid flux in the microporous matrix $\underline{q}$ is not triggered by the pore pressure p_p. Consequently, there is no apparent microporous fluid flow. Conversely, a low permeability contrast leads to identical fluid pressure fields in the microporous matrix and the pore domain. Actually, the case of interest is the intermediate situation. Then, both fluid fluxes coexist which means that the permeability contrast is not extremely high; and two pressure fields coexist which requires a high enough permeability contrast. We thus now analyse the fluid flows under this two pressure field regime. Because of the separation of scales, variations of pore pressure p_p are such that the pore pressure gradient at the macroscale is of order $O(p_p/L)$. Now, since $p = p_p$ over boundary Γ between the microporous matrix and the pore volume, a pressure gradient, of order $O(p/\ell) = O(p_p/\ell)$, exists within the matrix if p differs from p_p in the microporous domain. The existence of this local gradient induces a local transient regime and this means that the microporous domain is out of equilibrium. In other words, transient regimes simultaneously reached at both spatial scales suggest that the timescales are the same. On the other hand, the characteristic time of consolidation within the microporous matrix is given by:

$$\tau = O\left(2\pi\frac{\eta}{|B|}\frac{\ell^2}{\mathrm{K}}\right). \tag{3.5}$$

Therefore, equating both characteristic times τ and T leads to the following estimate of the permeability contrast

$$\frac{\mathrm{K}}{\mathrm{K}_p} = O((\ell/L)^2) = O(\varepsilon^2). \tag{3.6}$$

Hence, Darcy fluxes in the microporous and in the pore volume are respectively given by

$$|\underline{q}| = O\left(\mathrm{K}\frac{p}{\ell}\right), \qquad |\underline{q}_p| = O\left(\mathrm{K}_p\frac{p_p}{L}\right).$$

This allows concluding that the flux in the microporous matrix is one order of magnitude smaller than the flux in the pore domain:

$$|\underline{q}| = |\underline{q}_p| O\left(\frac{\mathrm{K}}{\mathrm{K}_p}\frac{p}{p_p}\frac{L}{\ell}\right) = O(\varepsilon|\underline{q}_p|) \tag{3.7}$$

Consequently, applying the homogenization procedure, we will consider the following asymptotic expansions for the fluxes:

$$\left.\begin{aligned} \underline{q}_p(\mathbf{x},\mathbf{y}) = -\frac{\mathbf{K}_p}{\eta}.\underline{\mathrm{grad}}(p_p) = \underline{q}_p^0(\mathbf{x},\mathbf{y}) + \varepsilon\underline{q}_p^1(\mathbf{x},\mathbf{y}) + \cdots \\ \underline{q}(\mathbf{x},\mathbf{y}) = -\frac{\varepsilon^2\mathbf{K}}{\eta}.\varepsilon^{-1}\underline{\mathrm{grad}}(p) = \varepsilon\underline{q}^1(\mathbf{x},\mathbf{y}) + \cdots \end{aligned}\right\} \tag{3.8}$$

The double porosity macroscopic behaviour is thus associated with the permeability ratio of eq. (3.6). Considering that both permeabilities can be estimated through the micropore a and pore a_p characteristic sizes as $\mathrm{K} = O(a^2)$ and $\mathrm{K}_p = O(a_p^2)$, the estimation (3.6) corresponds to the scale ratio $a/a_p = \varepsilon$. This is precisely the scale ratio considered in Auriault & Boutin (1993) to derive the double porosity model by a three scale homogenization approach.

We should also consider estimates associated with the constitutive law (3.2–b) for the fluid in the porous domain. The macroscopic pressure gradient must be balanced by viscous forces that vary at the pore scale:

$$\frac{P_p}{L} = O\left(\eta\frac{v_p}{a_p^2}\right).$$

This is a classical result of the normalization or rescaling procedure associated with the homogenization method of asymptotic expansions (Boutin & Auriault 1990; Auriault 1991). This leads to the classical rescaling of the constitutive law (3.2–b) (Auriault 1980):

$$\boldsymbol{\sigma}_p = -p_p\mathbf{I} + 2\eta\varepsilon^2\mathbf{D}(\underline{v}_p) \tag{3.9}$$

4 DOUBLE POROSITY POROELASTIC HOMOGENIZED DESCRIPTION

4.1 Main steps of homogenization process

Below, we summarize the main intermediate results of the homogenization procedure. The detailed developments of the problems of successive orders are reported in Appendix A. The leading order leads to uniform solid motion $\underline{U}(\underline{x})$ of the microporous matrix and to uniform pressure in the fluid-saturated porous domain $P_p(\underline{x})$. Then, the next problem in the pores is the usual local problem leading to Darcy's law. Thus, after averaging over the pore domain, it reads:

$$\phi_p(\underline{V}_p - i\omega\underline{U}) = -\frac{\mathbf{K}_p}{\eta}.\underline{\mathrm{grad}}_x(P_p), \tag{4.1}$$

where $\underline{V}_p$ is the mean fluid velocity in the pores and $\mathbf{K}_p$ denotes the tensor of intrinsic permeability related to the pore network. In the microporous domain Ω, the first order problem takes the form

$$\left.\begin{aligned} \underline{\mathrm{div}}_y\left(\mathbf{c} : (\mathbf{e}_x(\underline{U}) + \mathbf{e}_y(\underline{u}^1)) - \boldsymbol{\alpha}\, p^0\right) = \underline{0} \qquad & \text{in } \Omega \\ \left(\mathbf{c} : \left(\mathbf{e}_x(\underline{U}) + \mathbf{e}_y(\underline{u}^1)\right) - \boldsymbol{\alpha}\, p^0\right).\underline{n} = -P_p\underline{n} \qquad & \text{on } \Gamma \\ \mathrm{div}_y\left(\frac{\mathbf{K}}{\eta}.\underline{\mathrm{grad}}_y(p^0)\right) = i\omega\left[\boldsymbol{\alpha} : \left(\mathbf{e}_x(\underline{U}) + \mathbf{e}_y(\underline{u}^1)\right) + \frac{1}{M}p^0\right] \qquad & \text{in } \Omega \\ p^0 = P_p \qquad & \text{on } \Gamma \\ \underline{u}^1 \quad \text{and} \quad p^0, \quad \widehat{\Omega}-\text{periodic} & \end{aligned}\right\} \tag{4.2}$$

This differential set describes a non stationary local regime forced by both the macro deformation of the solid matrix $\mathbf{e}_x(\underline{U})$ and the pore pressure P_p. In Appendix A3.3, an analysis based on the definition of the particular local fields is carried out. It yields the following solution:

$$\left.\begin{aligned} \underline{u}^1 = \widetilde{\underline{u}} + \underline{u}_0^1 = (\underline{\boldsymbol{\xi}}_0(\underline{y}) + \widetilde{\underline{\boldsymbol{\xi}}}(\underline{y},\omega)) : \mathbf{e}_x(\underline{U}) - (\underline{\zeta}_0(\underline{y}) + \widetilde{\underline{\zeta}}(\underline{y},\omega))P_p, \\ p^0 = \widetilde{p} + P_p = \widetilde{\boldsymbol{\theta}}(\underline{y},\omega) : \mathbf{e}_x(\underline{U}) + (1 - \widetilde{\varpi}(\underline{y},\omega))P_p. \end{aligned}\right\} \tag{4.3}$$

In the above equations, the particular local fields are decomposed into their long-term part (i.e. when $\omega = 0$, namely, $\underline{\boldsymbol{\xi}}_0(\underline{y})$ and $\underline{\zeta}_0(\underline{y})$) and their transient part, namely, $\widetilde{\underline{\boldsymbol{\xi}}}(\underline{y},\omega)$, $\widetilde{\underline{\zeta}}(\underline{y},\omega)$, $\widetilde{\boldsymbol{\theta}}(\underline{y},\omega)$ and $\widetilde{\varpi}(\underline{y},\omega)$. We shall underline that both pressure fields differ, except at zero frequency

(i.e. at long term). We further note that the micropore pressure is not uniform, except at both limits of zero frequency (i.e. at long term) and of 'infinite'[1] frequency, (i.e. short term). In this latter case, a boundary layer arises at the pore/micropore interface Γ, which enables the sharp transition between both uniform pressure fields.

Finally, the macroscopic model is established by deriving the momentum and mass balances, from the local second order problems in both domains. Integrating the momentum balance over each volume, while accounting for the boundary condition and periodicity leads to the balance equation governing the macroscopic total stress tensor $\mathbf{S}$ in the double porosity medium:

$$\underline{\mathrm{div}}_x(\mathbf{S}) = 0, \qquad \mathbf{S} = \frac{1}{\widehat{\Omega}} \int_{\Omega} \mathbf{\Sigma}\, \mathrm{d}\Omega - \phi_p P_p \mathbf{I}, \tag{4.4}$$

where $\mathbf{\Sigma} = \mathbf{c} : (\mathbf{e}_x(\underline{U}) + \mathbf{e}_y(\underline{u}^1)) - \boldsymbol{\alpha}\, p^0$, and $\underline{u}^1$ and p^0 are given by (4.3). Hence, the constitutive law for the macroscopic total stress tensor reads:

$$\mathbf{S} = \mathbf{C}(\omega) : \mathbf{e}_x(\underline{U}) - \mathbf{A}(\omega) P_p. \tag{4.5}$$

Similarly, the macroscopic mass balance is obtained by integrating the mass balance over each volume, and by accounting for the boundary condition and periodicity. This leads to:

$$\phi_p \mathrm{div}_x\left(\underline{V}_p - i\omega \underline{U}\right) = i\omega \left(-\phi_p \left(\mathrm{div}_x(\underline{U}) + \frac{P_p}{K_f} \right) - \frac{1}{|\widehat{\Omega}|} \int_{\Omega} \left(\boldsymbol{\alpha} : (\mathbf{e}_y(\underline{u}^1) + \mathbf{e}_x(\underline{\mathrm{U}})) - \mathrm{div}_y(\underline{u}^1) + \frac{p^0}{M} \right) \mathrm{d}\Omega \right).$$

Replacing the local fields $(\underline{u}^1, p^0)$ by their expressions given by (4.3), the macroscopic mass balance governing the double porosity medium takes the form:

$$\phi_p \mathrm{div}_x(\underline{V}_p - i\omega \underline{U}) = i\omega \left(-\mathbf{B}(\omega) : \mathbf{e}_x(\underline{U}) - \frac{P_p}{\mathcal{M}(\omega)} \right). \tag{4.6}$$

4.2 Features of effective quantities

Effective tensors $\mathbf{C}(\omega)$, $\mathbf{A}(\omega)$, $\mathbf{B}(\omega)$ and scalar $1/\mathcal{M}(\omega)$ are directly related to the local particular fields and their expressions are given in Appendix A. In addition, the symmetry (minor and major) of the effective tensors $\mathbf{C}(\omega)$, $\mathbf{A}(\omega)$ and $\mathbf{B}(\omega)$, and the equality $\mathbf{A}(\omega) = \mathbf{B}(\omega)$ are established in Appendix B through the variational formulation of the local problems. This latter result reveals the symmetrical coupling between the pressure and solid deformation, even in a transient local regime. This is an erratum to the papers (Auriault & Boutin 1992, 1993), where a mistake on a volume integration led to the erroneous conclusion of non-symmetrical coupling in double porosity media.

The tensors $\mathbf{C}(\omega)$, $\mathbf{A}(\omega)$, and the scalar $1/\mathcal{M}(\omega)$ can be decomposed into elastic parts, $\mathbf{C}_0$, $\mathbf{A}_0$ and $1/\mathcal{M}_0$ that correspond to the long-term elastic response, and frequency-dependent parts $\widetilde{\mathbf{C}}(\omega)$, $\widetilde{\mathbf{A}}(\omega)$, and $1/\widetilde{\mathcal{M}}(\omega)$, that is,

$$\mathbf{C}(\omega) = \mathbf{C}_0 + \widetilde{\mathbf{C}}(\omega); \quad \mathbf{A}(\omega) = \mathbf{A}_0 + \widetilde{\mathbf{A}}(\omega); \quad \frac{1}{\mathcal{M}(\omega)} = \frac{1}{\mathcal{M}_0} + \frac{1}{\widetilde{\mathcal{M}}(\omega)}. \tag{4.7}$$

Furthermore, the analysis at low frequency shows that

$$\widetilde{\mathbf{C}}(\omega) \to i\eta\omega \mathbb{C}_0; \quad \widetilde{\mathbf{A}}(\omega) \to i\omega\eta \mathbb{A}_0; \quad \frac{1}{\widetilde{\mathcal{M}}(\omega)} \to \frac{i\omega\eta}{\mathbb{M}_0} \qquad \text{when} \qquad \omega \to 0, \tag{4.8}$$

where $\mathbb{C}_0$, $\mathbb{A}_0$ and $\mathbb{M}_0$ are frequency independent, dimensionless and real valued.

Alternatively, $\mathbf{C}(\omega)$, $\mathbf{A}(\omega)$ and $1/\mathcal{M}(\omega)$ can be decomposed into their elastic short-term parts (high-frequency limit, purely elastic, hence real) $\mathbf{C}_\infty$, $\mathbf{A}_\infty$ and $1/\mathcal{M}_\infty$ and frequency-dependent parts $\check{\mathbf{C}}(\omega)$, $\check{\mathbf{A}}(\omega)$ and $1/\check{\mathcal{M}}(\omega)$, that is:

$$\mathbf{C}(\omega) = \mathbf{C}_\infty + \check{\mathbf{C}}(\omega); \quad \mathbf{A}(\omega) = \mathbf{A}_\infty + \check{\mathbf{A}}(\omega); \quad \frac{1}{\mathcal{M}(\omega)} = \frac{1}{\mathcal{M}_\infty} + \frac{1}{\check{\mathcal{M}}(\omega)}. \tag{4.9}$$

The analysis of the behaviour at high-frequency shows that $\check{\mathbf{C}}(\omega)$, $\check{\mathbf{A}}(\omega)$ and $1/\check{\mathcal{M}}(\omega)$ account for the boundary-layer effect. Indeed, focusing on the isotropic case, we obtain

$$\check{\mathbf{C}}(\omega) \to \frac{\delta\Gamma}{\widehat{\Omega}} \mathbb{C}_\infty; \quad \check{\mathbf{A}}(\omega) \to \frac{\delta\Gamma}{\widehat{\Omega}} \mathbb{A}_\infty; \quad \frac{1}{\check{\mathcal{M}}(\omega)} \to \frac{\delta\Gamma}{\widehat{\Omega}} \frac{1}{\mathbb{M}_\infty} \qquad \text{when} \qquad \omega \to \infty. \tag{4.10}$$

In the above expressions, δ denotes the 'complex thickness' of the frequency-dependent boundary layer defined as

$$\delta = \sqrt{\frac{\mathrm{K}B}{i\omega\eta}}, \tag{4.11}$$

where K represents the isotropic microporous intrinsic permeability, B is the consolidation modulus and $\mathbb{C}_\infty$, $\mathbb{A}_\infty$ and $\mathbb{M}_\infty$ are frequency independent, dimensionless and real valued.

[1] Although 'infinite' frequencies are physically impossible, high-frequency regimes can be modelled by mathematically considering that $\omega \to \infty$. For simplicity, here and in the sequel, 'infinite' frequency indicates the high-frequency limit behaviour of the model.

4.3 Homogenized model

To summarize, and assuming the presence of harmonic macroscopic volume forces $\underline{\mathcal{F}}$ and of a harmonic density of fluid injection $\mathcal{V}$, the description of the double porosity medium in harmonic regime is given by the following set of equations, in which the index 0 indicating the leading order, and index x indicating the macroscale derivation have been omitted:

$$\left.\begin{aligned} \underline{\mathrm{div}}(\mathbf{S}) + \underline{\mathcal{F}} &= \underline{0} \\ \mathbf{S} = \mathbf{C}(\omega) : \mathbf{e}(\underline{U}) - \mathbf{A}(\omega) P_p &\\ \phi_p \,\mathrm{div}(\underline{V_p} - i\omega\underline{U}) + i\omega\mathcal{V} = i\omega\left(-\mathbf{A}(\omega) : \mathbf{e}(\underline{U}) - \frac{P_p}{\mathcal{M}(\omega)}\right) &\\ \phi_p(\underline{V_p} - i\omega\underline{U}) = -\frac{\mathbf{K}_p}{\eta}.\underline{\mathrm{grad}}(P_p) &\end{aligned}\right\} \tag{4.12}$$

This set is formally similar to the classical biphasic Biot model described by the motion of the macroporous domain $\underline{U}$ and the pressure P_p of the pore domain (as well as the mean fluid velocity $\underline{V_p}$ in the pores). However, due to the transient regime at the microporous scale, the effective tensor of stiffness $\mathbf{C}$, the coupling tensor $\mathbf{A}$ and the compressibility $\mathcal{M}$ are complex and frequency dependent. This corresponds to a Biot porous medium with a viscoelastic skeleton and where the fluid appears to be viscous Newtonian, but with a viscoelastic compressibility.

4.3.1 Memory effects and apparent viscoelasticity

In order to investigate these effects, we first separate the transient and long-term responses of $\mathbf{C}$, $\mathbf{A}$ and $\mathcal{M}$ by incorporating expressions (4.7) into the macroscopic description (4.12):

$$\left.\begin{aligned} \underline{\mathrm{div}}(\mathbf{S}) + \underline{\mathcal{F}} &= \underline{0} \\ \mathbf{S} = [\mathbf{C}_0 + \widetilde{\mathbf{C}}(\omega)] : \mathbf{e}(\underline{U}) - [\mathbf{A}_0 + \widetilde{\mathbf{A}}(\omega)] P_p &\\ \phi_p \,\mathrm{div}(\underline{V_p} - i\omega\underline{U}) + i\omega\mathcal{V} = -i\omega[\mathbf{A}_0 + \widetilde{\mathbf{A}}(\omega)] : \mathbf{e}(\underline{U}) - i\omega\left[\frac{1}{\mathcal{M}_0} + \frac{1}{\widetilde{\mathcal{M}}(\omega)}\right] P_p &\\ \phi_p(\underline{V_p} - i\omega\underline{U}) = -\frac{\mathbf{K}_p}{\eta}.\underline{\mathrm{grad}}(P_p) &\end{aligned}\right\} \tag{4.13}$$

Then, we come back to the time domain by inverse Fourier transform. We thus obtain the following integro-differential model with memory effects:

$$\left.\begin{aligned} \underline{\mathrm{div}}(\mathbf{S}_t) + \underline{\mathcal{F}}_t &= \underline{0} \\ \mathbf{S}_t = \mathbf{C}_0 : \mathbf{e}(\underline{U}_t) - \mathbf{A}_0 P_{pt} + \widehat{\widetilde{\mathbf{C}}}_t : \mathbf{e}(\underline{U}_t) - \widehat{\widetilde{\mathbf{A}}}_t * P_{pt} &\\ \phi_p \,\mathrm{div}(\underline{V_{pt}} - \underline{\dot{U}_t}) + \dot{\mathcal{V}}_t = -\mathbf{A}_0 : \mathbf{e}(\underline{\dot{U}_t}) - \frac{\dot{P}_{pt}}{\mathcal{M}_0} - \widehat{\widetilde{\mathbf{A}}}_t : \mathbf{e}(\underline{\dot{U}_t}) - \widehat{\widetilde{\mathcal{M}^{-1}}}_t * \dot{P}_{pt} &\\ \phi_p(\underline{V_{pt}} - \underline{\dot{U}_t}) = -\frac{\mathbf{K}_p}{\eta}.\underline{\mathrm{grad}}(P_{pt}) &\end{aligned}\right\} \tag{4.14}$$

where time-dependent variables are indexed by $_t$, and in which $\widehat{\widetilde{\mathbf{C}}}(t)$, $\widehat{\widetilde{\mathbf{A}}}(t)$ and $\widehat{\widetilde{\mathcal{M}}}(t)$ are defined by means of convolution products. For example

$$\widehat{\widetilde{\mathbf{C}}}(t) = \int_{-\infty}^{\infty} \widetilde{\mathbf{C}}(\omega)\exp(-i\omega t)\,\mathrm{d}\omega; \quad \widehat{\widetilde{\mathbf{C}}}(t) : \mathbf{e}(\underline{U}(t)) = \int_0^t \widehat{\widetilde{\mathbf{C}}}(\tau) : \mathbf{e}(\underline{U}(t-\tau))\,\mathrm{d}\tau.$$

The memory effects result in an apparent viscoelasticity, which induces both creep and relaxation phenomena. The assessment of the retardation effects requires the knowledge of local fields which are determined from the microstructure and the mechanical parameters of the constituents. In general, numerical methods are necessary to solve this local problem. However, some simple morphologies can be investigated analytically. Exact derivation can, indeed, be performed in the academic case of fluid/microporous stratified media as described in Section 7 ; and for the case of a medium made of spherical pores embedded in a microporous matrix can be investigated using a self-consistent/geometrical approximation approach. This latter problem is the subject of a subsequent paper.

The spectral decomposition described in Appendix A (Appendix A3.4) provides an alternative manner to account for the apparent viscoelastic effects without introducing convolution products. According to eqs (A29-a), (A43-a) and (A52-a) transposed in the time domain, the behaviour of the double porosity medium can be described as follows

$$\left.\begin{aligned}
\underline{\mathrm{div}}(\mathbf{S}_t)+\underline{\mathcal{F}}_t&=\underline{0}\\
\mathbf{S}_t&=\mathbf{C}_0:\mathbf{e}(\underline{U}_t)-\mathbf{A}_0P_{pt}+\sum_I a_{It}(\mathbf{s}_I-\boldsymbol{\alpha}\mathcal{P}_I)\\
\phi_p\mathrm{div}(\underline{U}_{pt}-\underline{U}_t)+\mathcal{V}_t&=-\mathbf{A}_0:\mathbf{e}(\underline{U}_t)-\frac{P_{pt}}{\mathcal{M}_0}-\sum_I a_{It}\left(\mathcal{B}_I+\frac{\mathcal{P}_I}{M_0}\right)\\
\phi_p(\dot{\underline{U}}_{pt}-\dot{\underline{U}}_t)&=-\frac{\mathbf{K}_p}{\eta}.\underline{\mathrm{grad}}(P_{pt})\\
\frac{\kappa_I}{\eta}a_{It}+\left(\frac{1}{M}+D_{II}\right)\dot{a}_{It}+\sum_{J\neq I}D_{IJ}\dot{a}_{Jt}&=-\left(\mathbf{D}_I:\mathbf{e}_x(\dot{\underline{U}}_t)+\mathcal{D}_I\frac{\dot{P}_{pt}}{M}\right)
\end{aligned}\right\} \tag{4.15}$$

where $\mathbf{s}_I, \mathcal{P}_I, \mathcal{B}_I, D_{IJ}, \mathcal{D}_I, \mathbf{D}_I$ are defined in (A29-b), (A43-b) and (A52-b).

In this form, the additional variables $a_I(\underline{x},t)$ are the instantaneous amplitudes of eigenfunctions corresponding to microscopic descriptors. They are introduced instead of keeping only the macroscopic variables $\underline{U}$ and P_p, which require to deal with convolution products. Thus, both the microscopic descriptors and macro variables can be determined in parallel by solving the coupled linear differential set governing their time/space evolution. Such a formulation is usual in the framework of generalized continua where the microstructural effects are 'condensed' into additional variables governed by specific equations of evolution (Eringen 1968; dell'Isola *et al.* 1997a). The multiscale identification method (dell'Isola *et al.* 1997b) based on the identification of micro and macro Lagrangians and on suitable micro-macro correspondence of kinematical descriptors is somehow similar to the spectral approach.

The formulation in terms of microscopic descriptors may be convenient for computational methods (see for example, Liu *et al.* 2009; Carcione *et al.* 2010). In fact, the use of microscopic descriptors (i) avoids the difficulties associated to the numerical treatment of convolution products, which requires to store the data of the preceding steps of calculation Arbogast (1997), (ii) does not require multi-scale mesh, conversely to the 'square' finite element method (FEM^2). In fact, local fields are pre-integrated within parameters $\mathbf{s}_I, \mathcal{P}_I, \mathcal{B}_I, D_{IJ}, \mathcal{D}_I, \mathbf{D}_I$, which are determined from the eigenmodes calculations in the microporous domain. Furthermore, the relevant number of eigenmodes required for the calculations can be adapted according to the frequency spectrum content. Double porosity media differ from 'standard' generalized continua, mainly by the fact that the time evolution of each microscopic descriptor is ruled by differential equations of the first order, with a forcing term related to the macroscopic variables. Consequently, the descriptors can formally be determined as a function of the macro variables and their combination constitutes the kernel of the convolution product. For this reason, $a_I(\underline{x},t)$ are hidden variables in the usual description formulated in terms of the macroscopic variables $\underline{U}$ and P_p only.

The kernel of the convolution product can be explicitly expressed when the eigenmodes are fully decoupled (i.e. not only for pressure but also for the associated motions). In that case, $D_{IJ}=D_I\delta_{IJ}$ and the amplitudes a_I satisfy:

$$\frac{\kappa_I}{\eta}a_{It}+\left(\frac{1}{M}+D_{II}\right)\dot{a}_{It}=-\left(\mathbf{D}_I:\mathbf{e}_x(\dot{\underline{U}}_t)+\mathcal{D}_I\frac{\dot{P}_{pt}}{M}\right). \tag{4.16}$$

Hence, the free time variation of a_{It} is an exponential decay of characteristic time

$$\tau_I=\left(\frac{1}{M}+D_{II}\right)\frac{\eta}{\kappa_I}=O\left(\left(\frac{1}{M}+\frac{1}{|\mathbf{c}|}\right)\frac{\ell^2\eta}{|\mathbf{K}|I}\right)=O\left(\frac{\ell^2\eta}{|\mathbf{K}|BI}\right)$$

and integrating leads to

$$a_I(\underline{x},t)=\frac{1}{\frac{1}{M}+D_{II}}\int_{-\infty}^{t}-\exp\left(-\frac{t-u}{\tau_I}\right)\left[\mathbf{D}_I:\mathbf{e}_x(\dot{\underline{U}}_u)+\mathcal{D}_I\frac{\dot{P}_{pu}}{M}\right]\mathrm{d}u. \tag{4.17}$$

This shows that the kernel of the convolution product is the sum of the impulse responses of each amplitude a_I. According to the characteristic time of variation t_c of the macroscopic variables, a_I simplifies into:

$$\left.\begin{aligned}
a_I(\underline{x},t)&\approx-\frac{\eta}{\kappa_I}\left(\mathbf{D}_I:\mathbf{e}_x(\dot{\underline{U}}_t)+\mathcal{D}_I\frac{\dot{P}_{pt}}{M}\right)\qquad\text{if}\qquad t_c\gg\tau_I\\
a_I(\underline{x},t)&\approx-\frac{1}{\frac{1}{M}+D_{II}}\left(\mathbf{D}_I:\mathbf{e}_x(\underline{U}_t)+\mathcal{D}_I\frac{P_{pt}}{M}\right)\qquad\text{if}\qquad t_c\ll\tau_I
\end{aligned}\right\} \tag{4.18}$$

4.3.2 Case of a rigid skeleton

In case of a rigid skeleton, or of a skeleton with a modulus much larger than the fluid bulk modulus, then the solid motion vanishes and the description reduces to the combination of a simplified mass balance with Darcy's law. Eliminating the flux, and in the absence of a source

term, the description becomes:

$$\operatorname{div}\left(\frac{\mathbf{K}_p}{\eta}.\underline{\operatorname{grad}}(P_p)\right) = \left(\frac{\phi_p}{K_f} + \frac{\varphi}{K_f} + \frac{1}{\widetilde{\mathcal{M}}(\omega)}\right) i\omega P_p \tag{4.19}$$

where $\varphi = \phi(1-\phi_p)$ and M reduces to K_f/ϕ_p.

Using the spectral decomposition, the description can be rewritten as:

$$\left.\begin{aligned} \operatorname{div}\left(\frac{\mathbf{K}_p}{\eta}.\underline{\operatorname{grad}}(P_{pt})\right) &= \dot{P}_{pt}\frac{\phi_p+\varphi}{K_f} + \frac{\phi}{K_f}\sum_I a_{It}\mathcal{P}_I \\ a_{It} + \frac{\eta\phi}{K_f\kappa_I}\dot{a}_{It} &= -\frac{\eta\phi\mathcal{D}_I}{K_f\kappa_I}\dot{P}_{pt} \end{aligned}\right\} \tag{4.20}$$

5 TIMESCALE RATIO VERSUS PERMEABILITY CONTRAST AS KEY PARAMETER FOR PREDICTING DOUBLE POROSITY EFFECTS

As already noticed in pioneering works Auriault (1983) and Arbogast (1989), the order of magnitude of the thermal conductivity or of the permeability contrast that gives rise to a macroscopic model with two interacting fields is: $\frac{\mathrm{K}}{\mathrm{K}_p} = O(\varepsilon^2)$. Following the reasoning adopted in Section 3.5, a higher contrast, that is, $\frac{\mathrm{K}}{\mathrm{K}_p} \leq O(\varepsilon^3)$ implies that the micropore fluid flux is smaller than the pore fluid flux by two orders of magnitude $|\underline{q}| \leq O(\varepsilon^2|\underline{q}_p|)$. As a consequence, the micropore fluid flux at the local scale is too small to balance the volume variation of the microporous domain. Hence, instead of eq. (4.2-c) we have

$$0 = i\omega\left[\boldsymbol{\alpha} : \left(\mathbf{e}_x(\underline{U}) + \mathbf{e}_y(\underline{u}^1)\right) + \frac{1}{M}p^0\right] \tag{5.1}$$

which leads to the same description as that obtained for the high-frequency case.

Conversely, a weaker contrast, that is, $\frac{\mathrm{K}}{\mathrm{K}_p} \geq O(\varepsilon)$, facilitates the fluid flux in the micropores, so that the pressure gradient in the microporous domain is of the same order of magnitude as that in the pore volume. Consequently, the flux is estimated as

$$|\underline{q}| = O\left(\mathrm{K}\frac{p}{L}\right)$$

Furthermore, the fluid flow gives now rise to macroscopic volume variations of the medium. These are greater by one order of magnitude than both the volume variation due to solid deformation and the fluid compressibility. Hence, the mass balance of the Biot model is rescaled as follows:

$$\operatorname{div}(\underline{q}) = \varepsilon\left[-\boldsymbol{\alpha} : \mathbf{e}(\dot{\underline{u}}) - \frac{\dot{p}}{M}\right] \qquad \text{with} \qquad \underline{q}(\mathbf{x},\mathbf{y}) = -\frac{\varepsilon\mathbf{K}}{\eta}.\underline{\operatorname{grad}}(p) = \varepsilon\underline{q}^1(\mathbf{x},\mathbf{y}) + \cdots$$

In this situation, the local scale eq. (4.2-c), is replaced by

$$\operatorname{div}_y\left(\frac{\mathbf{K}}{\eta}.\underline{\operatorname{grad}}_y(p^0)\right) = 0 \tag{5.2}$$

which, together with the associated boundary conditions, leads to $p^0 = P_p$, and therefore to the low-frequency description.

As discussed for similar problems in Royer & Boutin (2012) (see also Boutin *et al.* 1998), this analysis shows that the order of magnitude of the permeability ratio is in fact linked to the temporal regime experienced by the microporous domain. This regime is determined by the ratio of the intrinsic characteristic time of consolidation in the microporous domain, τ *cf.* eq. (3.5), to the macroscopic characteristic time T of the considered phenomenon. Consider a 'two permeability' medium with a *given* value of permeability contrast $\frac{\mathrm{K}}{\mathrm{K}_p} < 1$. The behaviour is conditioned by the timescale ratio:

(1) if $T/\tau = O(1)$: the double porosity model (4.12) with memory (or viscoelastic) effects applies. In this case, both the microporous and the macroscopic domains experience a transient regime and two distinct and interacting pressure fields coexist.

(2) if $T/\tau \gg O(1)$: the low-frequency limit of the double porosity model applies. The microporous matrix behaves locally as a Biot medium in drained condition, but remains in quasi-static state regime, while the macro domain experiences a transient regime. The pore and the macropore domains undergo the same pressure, and the behaviour is described by Biot's model, but with the elastic effective properties of the dry double porosity structure.

(3) if $T/\tau \ll O(1)$, the high-frequency limit of the double porosity model applies. In this situation, the fluid in the micropores has not enough time to flow throughout the medium. Hence, the microporous domain is unable to be excited and behaves locally as a Biot medium in undrained condition, while the macro domain experiences a transient flow regime. Macroscopically, the medium is described by a Biot model whose effective elastic tensor takes into account the fact that the microporous domain is saturated by a static fluid.

These definitions of the model domains of validity trough the timescale ratio are consistent with those deduced from the permeability contrasts, which are intrinsically linked to length scales. As previously mentioned, T is associated to the macroscopic characteristic length $L = \varepsilon^{-1}\ell$ by

$$T = O\left(2\pi \frac{\eta}{|B|}\frac{L^2}{\mathrm{K}_p}\right) \quad \text{thus} \quad \frac{T}{\tau} = \frac{\mathrm{K}}{\mathrm{K}_p}\frac{L^2}{\ell^2}. \tag{5.3}$$

Hence, for a given dual permeability medium, the following orders of magnitude of the permeability contrast $\frac{\mathrm{K}}{\mathrm{K}_p} \gg O(\varepsilon^2)$, $\frac{\mathrm{K}}{\mathrm{K}_p} = O(\varepsilon^2)$, $\frac{\mathrm{K}}{\mathrm{K}_p} \ll O(\varepsilon^2)$, will lead to the slow, $T/\tau \ll O(1)$, the intermediate, $T/\tau = O(1)$, and the fast, $T/\tau \gg O(1)$ evolutions, respectively. The slow and fast variations are the limit cases of the intermediate description. However, for extremely slow variations the permeability contrast appears to be $O(1)$. In this case the effective permeability should include the flow in the microporous domain, regardless of its small magnitude.

6 HOMOGENIZED VERSUS PHENOMENOLOGICAL MODELS

Although homogenized and phenomenological models—as in Barenblatt *et al.* (1960) (herein after denoted 'BZK') or in Warren & Root (1963) ('WR')—both involve two distinct pressure fields, both types of models are strongly distinct, as already noticed in Hornung & Showalter (1990), Auriault & Royer (1993), Royer & Auriault (1994) and Royer *et al.* (1996). As neither the skeleton elasticity, nor the possible anisotropy are essential factors for the pressure regime, it is sufficient to focus on rigid isotropic porous media for analysing this mismatch. Therefore, throughout this section we assume $B = M = K_f/\phi_p$.

In the homogenization method, the micro morphology of double porosity media is explicitly described and the corresponding family of models, according to the permeability contrast value, is rigorously established. Now, regardless of the up-scaling procedure, identical microscopic morphologies must lead to the same macroscopic behaviour. Consequently, and conversely to the widely accepted postulate, the BZK and WR models *do not* correspond to the same double porosity / double permeability morphology as that derived by homogenization. In fact, since the phenomenological models are directly stated at the macro scale, by principle, one can only conjecture the micromorphology that these models are able to describe.

A relevant micro morphology responding to the phenomenological models can be identified, if, when treated by homogenization, a description identical to the phenomenological models is obtained. Let us remind the BZK formulation expressed in the frequency domain (with similar notations as in this paper, and s being an undetermined area parameter)

$$\left.\begin{aligned} \frac{\mathrm{K}_p}{\eta}\Delta P_p &= \frac{\phi_p}{K_f} i\omega P_p - \frac{\mathrm{K}}{s\eta}(P - P_p) \\ \frac{\mathrm{K}}{\eta}\Delta P &= \frac{\varphi}{K_f} i\omega P + \frac{\mathrm{K}}{s\eta}(P - P_p) \end{aligned}\right\} \tag{6.1}$$

Transposed to thermal conduction problems, the BZK model corresponds to composites with high thermal contact resistance as studied in Auriault & Ene (1994). The BZK model incorrectly describes double porosity media, as defined in this paper. However, it is correct in describing a medium with two pore networks, with permeabilities K and K_p, and porosities φ, ϕ_p of the same order, separated by a thin layer of thickness e of much lower permeability k, see Auriault *et al.* (2009). This is illustrated in Fig. 2. After homogenization, this inner interface gives rise to (i) the coexistence of two macroscopic uniform fields of pressure, and (ii) a flux between the two networks driven by the difference of pressure $P - P_p$ and an effective parameter $\frac{\mathrm{K}}{s} = O(\frac{\Gamma k}{e\Omega})$, see Royer & Auriault (1999) for the case of transfer of compressible

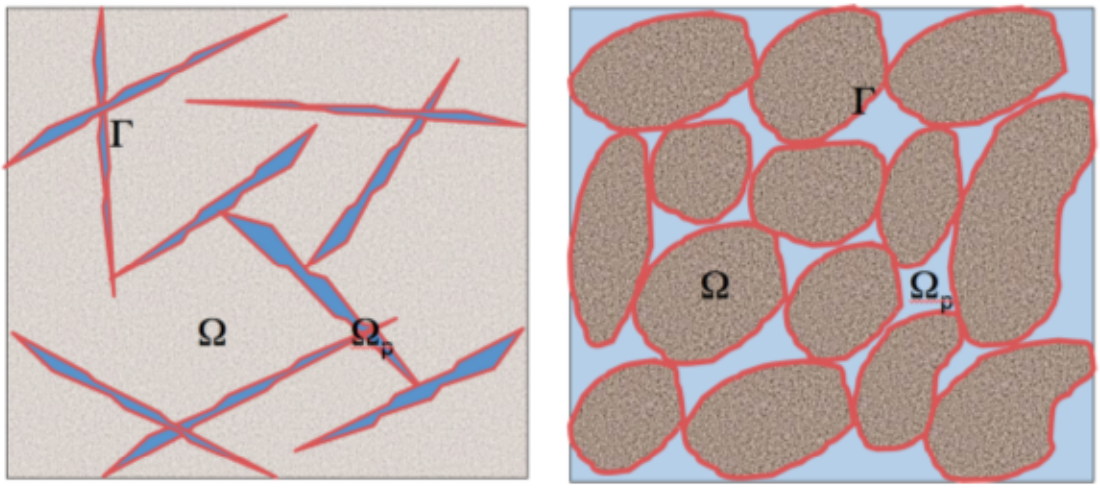

Figure 2. Elementary representative volume $\widehat{\Omega}$ corresponding to BZK and WR phenomenological models. Left: fissured microporous material. Right: microporous medium with pore network. In both cases the microporous domains are separated from the pore (or fissure) domain by a thin layer of high hydraulic resistivity on Γ.

gas. In this model both networks play symmetrical roles which is not consistent with the assumption of contrasted permeabilities. For this reason, in the WR model the smallest permeability is discarded and set to zero. Therefore, the pressure in the more permeable network forces the pressure in the less permeable one.

$$\left.\begin{aligned}\frac{\mathrm{K}_p}{\eta}\triangle P_p &= \frac{\phi_p}{K_f} i\omega P_p - \frac{\mathrm{K}}{s\eta}(P-P_p)\\ 0 &= \frac{\varphi}{K_f} i\omega P + \frac{\mathrm{K}}{s\eta}(P-P_p)\end{aligned}\right\} \tag{6.2}$$

As the BZK model, the WR model (and its extensions to poroelasticity) would rigorously be obtained by homogenization for media having two pore networks, but with contrasted permeabilities (i.e. $\mathrm{K} \ll \mathrm{K}_p$), separated by a thin layer of much smaller permeability. Two distinct uniform pressures coexist at the local scale with an inner flow between the two networks. With this morphology the area parameter s is in the order of $s = O(\frac{e\widehat{\Omega}}{\Gamma}\frac{K}{k})$.

Despite the permeability contrast, this micro morphology also differs from that of double porosity media. Nevertheless, due to the unsymmetrical role of the pressures, the WR model is 'closer' to the double porosity model than the BZK model. In addition, at low frequency $P \to P_p$ and at high-frequency $P \to 0$ which is also consistent with the homogenized model. Besides, we can eliminate pressure P to obtain

$$\frac{\mathrm{K}_p}{\eta}\triangle P_p = \left(\frac{\phi_p}{K_f} + \frac{1}{\frac{K_f}{\varphi} + i\omega\eta\frac{s}{\mathrm{K}}}\right) i\omega P_p. \tag{6.3}$$

This form enables a direct comparison with the homogenized double porosity model (4.19). An exact match would be obtained if the terms $(\frac{K_f}{\varphi} + i\omega\eta\frac{s}{\mathrm{K}})^{-1}$ and $\frac{\varphi}{K_f} + \frac{1}{\mathcal{M}(\omega)}$ were equal in the whole frequency range.

At low frequency, as M simplifies into $\frac{K_f}{\varphi}$, according to the results of Appendix A5

$$\frac{\varphi}{K_f} + \frac{1}{\widetilde{\mathcal{M}}} \approx \frac{\varphi}{K_f}\left[1 + \frac{i\omega\eta}{K_f}\frac{\varphi\Gamma\sigma_0}{\mathrm{K}}\right] \qquad \text{when} \qquad \omega \to 0 \tag{6.4}$$

where σ_0 is a dimensionless parameter $O(1)$ determined from the low-frequency local problem (*cf.* Appendix A3.5), and Γ is the area of the pores/microporous domain interface. Thus, at low frequency, a match at the first and second order can be obtained by setting the undetermined area parameter of the WR model to $s = \sigma_0\Gamma$. With this approximation, both models expressed in the time domain reduce to

$$\frac{\mathrm{K}_p}{\eta}\triangle P_p \approx \frac{1}{K_f}\left((\phi_p+\varphi)\partial_t P_p + \varphi\frac{\eta}{K_f}\frac{\varphi\Gamma\sigma_0}{\mathrm{K}}\partial_{tt} P_p\right). \tag{6.5}$$

This low-frequency representation is valid in the frequency range $\omega \ll 2\pi/\tau = O(\frac{K_f\mathrm{K}}{\eta\phi_p\Gamma})$

At high-frequency, that is, when $\omega \to \infty$, we have, respectively, and according to the results of Appendix A5 (σ_∞ is a dimensionless parameter $O(1)$):

$$\left.\begin{aligned}\left(\frac{K_f}{\varphi} + i\omega\eta\frac{s}{\mathrm{K}}\right)^{-1} &\approx \frac{\mathrm{K}}{i\omega\eta s}\\ \frac{\varphi}{K_f} + \frac{1}{\widetilde{\mathcal{M}}} &\approx \frac{\varphi}{K_f}\sqrt{\frac{K_f}{i\omega\eta}}\sqrt{\frac{\mathrm{K}}{\varphi}}\frac{\Gamma\sigma_\infty}{\widehat{\Omega}}\end{aligned}\right\} \tag{6.6}$$

Because of the frequency dependence in $1/\omega$ instead of $1/\sqrt{\omega}$, the WR model cannot match the homogenized double porosity model. Hence, the WR description provides erroneous description of double porosity media for frequencies $\omega \geq O(\frac{K_f\mathrm{K}}{\phi_p\eta\Gamma})$. This comes from the fact that the flux between the two networks is in general not instantaneous as assumed in the WR model. The reader can refer to Auriault & Royer (1993) where an improvement at low frequency of the WR is proposed through a time-dependent transfer law. For the whole frequency range, the only way to reach a perfect match between both approaches would be to introduce a frequency-dependent transfer parameter $\frac{s(\omega)}{\mathrm{K}}$ such that

$$i\omega\eta\frac{s(\omega)}{\mathrm{K}} = \left(\frac{\varphi}{K_f} + \frac{1}{\widetilde{\mathcal{M}}}\right)^{-1} - \frac{K_f}{\varphi}. \tag{6.7}$$

It is pertinent to remind that function $\widetilde{\mathcal{M}}(\omega)$ is specific to each morphology. However, its determination can be simplified by observing that the kernel doesn't present poles on the real axis, and $\widetilde{\mathcal{M}}$ is therefore a smooth continuous function. Thus, from calculations at low and high-frequency only, a reliable expression for the whole frequency range can be approximated in the following form, that matches the low and high frequencies behaviours:

$$\widetilde{\mathcal{M}}(\omega) = \frac{\varphi}{K_f}\left[1 + \frac{\sqrt{1+i\omega^*/\mathrm{F}^2}}{i\omega^*}\right]; \qquad \omega^* = \frac{\omega^*}{\omega_{dp}},$$

where the critical frequency ω_{dp} separating the low- and high-frequency behaviour of the double porosity medium, and the dimensionless form factor $\mathbb{F}$ are defined by

$$\omega_{dp} = \frac{K_f}{\eta}\frac{\mathrm{K}}{\varphi\Gamma\sigma_0}; \qquad \mathbb{F} = \frac{\widehat{\Omega}}{\sqrt{|\Gamma|^3\sigma_0\sigma_\infty}}.$$

Finally, the possibility of matching the homogenized and WR models applies only for the pressure field in the pores and the mean flux stem from the microporous domain. However, the pressure in the microporous domain is uniform in the WR model while it is non-uniform in the homogenized model. Consequently, in the case of elastic skeleton, the WR model cannot take into account the consolidation within the microporous domain, which requires an inhomogeneous pressure. Hence, the viscoelastic effect cannot be described when adopting the WR model for the fluid transfer, as it is done in most of the phenomenological double porosity poroelastic models (see for example Wilson & Aifantis 1982, 1984).

7 STRATIFIED DOUBLE POROSITY MEDIA

To illustrate the viscoelastic properties of double porosity media, consider now the simple case of a stratified periodic medium. This is made of parallel layers of an isotropic microporous material, of thickness $h = (1-\phi_p)\ell$, separated by fluid layers of thickness $\phi_p\ell$. The normal of the layers is oriented along the y_2-axis (or equivalently x_2-axis) and, because of the invariance along y_1 and y_3 axes, the local fields depend only on y_2. The fluid layer undergoes a pressure P_p. According to the plane geometry, y_1 and y_3 play the same role. Therefore, we investigate the response under macroscopic in plane kinematics defined by $\underline{U} = U_1(x_1, x_3)\underline{a}_1$. It corresponds to the macroscopic strain tensor involving both volumetric (E_{11}) and deviatoric strains (E_{13}):

$$\mathbf{e}_x(\underline{U}) = \begin{pmatrix} E_{11} & 0 & E_{13} \\ 0 & 0 & 0 \\ E_{13} & 0 & 0 \end{pmatrix}. \tag{7.1}$$

Because of the local invariance along y_1 and y_3 axes, the local fields depend only on y_2, that is, $\underline{u}^1 = u_i^1(y_2)\underline{a}_i$, and

$$\mathbf{e}_y(\underline{u}^1) = \begin{pmatrix} 0 & \frac{1}{2}u^1_{1,2} & 0 \\ \frac{1}{2}u^1_{1,2} & u^1_{2,2} & \frac{1}{2}u^1_{3,2} \\ 0 & \frac{1}{2}u^1_{3,2} & 0 \end{pmatrix}. \tag{7.2}$$

Thus, the effective stress $\boldsymbol{\sigma}^0(x_1, y_2, x_3)$ in the microporous skeleton reads:

$$\boldsymbol{\sigma}^0 = \lambda(E_{11} + u^1_{2,2})\mathbf{I} + 2\mu \begin{pmatrix} E_{11} & \frac{1}{2}u^1_{1,2} & E_{13} \\ \frac{1}{2}u^1_{1,2} & u^1_{2,2} & \frac{1}{2}u^1_{3,2} \\ E_{13} & \frac{1}{2}u^1_{3,2} & 0 \end{pmatrix}. \tag{7.3}$$

7.1 Long-term and short-term behaviours

Consider the local problem (A6), defined in Appendix A3.1 and which describes the long-term (or zero-frequency) response. The momentum balance equation $\underline{\mathrm{div}}(\boldsymbol{\sigma}^0_0) = \underline{0}$ leads to:

$$\sigma^0_{0i2,2} = 0; \quad i = 1, 2, 3.$$

Now, using the boundary condition we derive the constant values

$$\sigma^0_{012} = \sigma^0_{032} = 0; \quad \sigma^0_{022} = (-1+\alpha)P_p.$$

Consequently, we obtain:

$$u^1_{01,2} = u^1_{03,2} = 0; \quad u^1_{02,2} = -\frac{\lambda}{\lambda+2\mu}E_{11} - \frac{1-\alpha}{\lambda+2\mu}P_p.$$

This implies that for this stratified medium, we have:

$$\underline{\xi}^{11}_0 = -\frac{\lambda}{\lambda+2\mu}y_2\underline{a}_2; \quad \underline{\xi}^{13}_0 = \underline{0}; \quad \underline{\zeta}_0 = \frac{1-\alpha}{\lambda+2\mu}y_2\underline{a}_2.$$

The macroscopic total stress tensor reads:

$$\mathbf{S} = (1-\phi_p)(\boldsymbol{\sigma}^0 - \alpha \mathbf{I} P_p) - \phi_p \mathbf{I} P_p \tag{7.4}$$

and the non-zero components are

$$S_{11} = (1-\phi_p)\left(\lambda \frac{2\mu}{\lambda+2\mu} + 2\mu\right) E_{11} - \left(1 + (\alpha-1)\frac{2\mu}{\lambda+2\mu}\right) P_p,$$

$$S_{22} = -P_p,$$

$$S_{33} = (1-\phi_p)\lambda \frac{2\mu}{\lambda+2\mu} E_{11} - \left(1 + (\alpha-1)\frac{2\mu}{\lambda+2\mu}\right) P_p,$$

$$S_{13} = S_{31} = (1-\phi_p) 2\mu E_{13}.$$

Hence, the effective parameters at low frequency read:

$$\left.\begin{aligned} \mathbf{C}_0|_{11}^{11} = (1-\phi_p) 4\mu \frac{\lambda+\mu}{\lambda+2\mu}; \quad \mathbf{C}_0|_{22}^{11} = 0 \\ \mathbf{C}_0|_{33}^{11} = (1-\phi_p) 2\mu \frac{\lambda}{\lambda+2\mu}; \quad \mathbf{C}_0|_{13}^{13} = (1-\phi_p) 2\mu \\ \mathbf{A}_0|_{11} = \mathbf{A}_0|_{33} = 1 - (1-\phi_p)(1-\alpha)\frac{2\mu}{\lambda+2\mu}; \quad \mathbf{A}_0|_{22} = 1 \\ \frac{1}{\mathcal{M}_0} = \frac{\phi_p}{K_f} + (1-\phi_p)\left(\frac{1}{M} + \frac{(1-\alpha)^2}{\lambda+2\mu}\right) \end{aligned}\right\} \tag{7.5}$$

Following the reasoning adopted in Appendix A3.2, the short-term behaviour can be derived in a similarly way, by changing c into $\mathbf{c} + M\boldsymbol{\alpha} \otimes \boldsymbol{\alpha}$ and modifying the forcing pressure by $\mathbf{I} - \boldsymbol{\alpha}$ in eq. (A6). In the isotropic case, this means that the Lamé coefficient λ becomes $\lambda_\infty = \lambda + \alpha^2 M$, and that the forcing pressure is reduced by a factor $1-\alpha$. Consequently, the effective parameters at high frequency read:

$$\left.\begin{aligned} \mathbf{C}_\infty|_{11}^{11} = (1-\phi_p) 4\mu \frac{\lambda_\infty+\mu}{\lambda_\infty+2\mu}; \quad \mathbf{C}_\infty|_{22}^{11} = \mathbf{C}_0|_{22}^{11} = 0 \\ \mathbf{C}_\infty|_{33}^{11} = (1-\phi_p) 2\mu \frac{\lambda_\infty}{\lambda_\infty+2\mu}; \quad \mathbf{C}_\infty|_{13}^{13} = \mathbf{C}_0|_{13}^{13} = (1-\phi_p) 2\mu \\ \mathbf{A}_\infty|_{11} = \mathbf{A}_\infty|_{33} = 1 - (1-\phi_p)\frac{2\mu}{\lambda_\infty+2\mu}; \quad \mathbf{A}_\infty|_{22} = 1 \\ \frac{1}{\mathcal{M}_\infty} = \frac{\phi_p}{K_f} + \frac{1-\phi_p}{\lambda_\infty+2\mu} \end{aligned}\right\} \tag{7.6}$$

Note that the response under macroscopic shear is identical at both short and long terms, since the pressure does not interact with the deviatoric part of strains.

7.2 Frequency-dependent behaviour

Consider the local problem (A17) defining the response $(\widetilde{\underline{u}}, \widetilde{p})$ at any frequency. In the stratified case with in-plane kinematics $\underline{U} = U_1(x_1, x_3)\underline{a}_1, y_2$ is the single variable. The differential set of equations thus becomes:

$$\left.\begin{aligned} (\lambda+2\mu)\widetilde{u}_{2,22} - \alpha \widetilde{p}_{,2} = 0; \quad \mu\widetilde{u}_{1,22} = \mu\widetilde{u}_{3,22} = 0 \qquad \text{for } |y_2| \le h/2 \\ (\lambda+2\mu)\widetilde{u}_{2,2} - \alpha\widetilde{p} = 0; \quad \mu\widetilde{u}_{1,2} = \mu\widetilde{u}_{3,2} = 0 \qquad \text{for } y_2 = \pm h/2 \\ \frac{\mathbf{K}}{i\omega\eta}\widetilde{p}_{,22} - \alpha\widetilde{u}_{2,2} - \frac{\widetilde{p}}{M} = \alpha\left(1 - \frac{\lambda}{\lambda+2\mu}\right) E_{11} + \left(\alpha\frac{\alpha-1}{\lambda+2\mu} + \frac{1}{M}\right) P_p \qquad \text{for } |y_2| \le h/2 \\ \widetilde{p} = 0 \qquad \text{for } y_2 = \pm h/2 \end{aligned}\right\} \tag{7.7}$$

Using the isotropy of $\boldsymbol{\alpha}$ and the fact that $\underline{u}_0^1 = \underline{\xi}_0^{11} E_{11} - \underline{\zeta}_0 P_p$, the term $\boldsymbol{\alpha} : (\mathbf{e}_x(\underline{U}) + \mathbf{e}_y(\underline{u}_0^1))$ simplifies into:

$$\alpha(\mathrm{div}_x(\underline{U}) + \mathrm{div}_y(\underline{\xi}_0^{11} E_{11} - \underline{\zeta}_0 P_p)) = \alpha\left(1 - \frac{\lambda}{\lambda+2\mu}\right) E_{11} + \alpha\frac{\alpha-1}{\lambda+2\mu} P_p$$

From (7.7–a,b), we deduce that $\widetilde{u}_1 = \widetilde{u}_3 = 0$ and that $(\lambda + 2\mu)\widetilde{u}_{2,2} = \alpha\widetilde{p}$. This latter relation substituted in (7.7–c) gives the following governing equation for pressure $\widetilde{p}$, where we shall remind that $\frac{1}{B} = \frac{1}{M} + \frac{\alpha^2}{\lambda+2\mu}$:

$$\frac{\mathrm{K}}{i\omega\eta}\widetilde{p}_{,22} - \frac{\widetilde{p}}{B} = \mathcal{D}(\underline{x}); \quad \mathcal{D}(\underline{x}) = \alpha\left(1 - \frac{\lambda}{\lambda+2\mu}\right)E_{11} + \left(\alpha\frac{\alpha-1}{\lambda+2\mu} + \frac{1}{M}\right)P_p.$$

Integration of this equation with boundary conditions (7.7–d) gives:

$$\widetilde{p}(y_2) = -\mathcal{D}(\underline{x})Bf'(y_2); \quad f'(y_2) = 1 - \frac{\cosh(y_2/\delta)}{\cosh(h/(2\delta))}; \quad \delta = \sqrt{\frac{\mathrm{K}B}{i\omega\eta}}.$$

Coming back to the expression of $\mathcal{D}$, we derive

$$\widetilde{\theta}^{11} = -\alpha B\left(1 - \frac{\lambda}{\lambda+2\mu}\right)f'(y_2); \quad \widetilde{\theta}^{13} = 0; \quad \widetilde{\varpi} = B\left(\alpha\frac{\alpha-1}{\lambda+2\mu} + \frac{1}{M}\right)f'(y_2).$$

Integrating equality $(\lambda + 2\mu)\widetilde{u}_{2,2} = \alpha\widetilde{p}$ gives the associated local displacement field

$$\underline{\widetilde{\xi}}^{11} = -\frac{\alpha^2 B}{\lambda+2\mu}\left(1 - \frac{\lambda}{\lambda+2\mu}\right)f(y_2)\underline{a}_2; \quad \underline{\widetilde{\xi}}^{13} = \underline{0}; \quad \underline{\widetilde{\zeta}} = \frac{\alpha B}{\lambda+2\mu}\left(\alpha\frac{\alpha-1}{\lambda+2\mu} + \frac{1}{M}\right)f(y_2)\underline{a}_2,$$

in which

$$f(y_2) = y_2 - \delta\frac{\sinh(y_2/\delta)}{\cosh(h/(2\delta))},$$

and thus

$$F(\omega) = \frac{1}{h}\int_{-h/2}^{h/2} f'(y_2)\,dy_2 = 1 - \frac{2\delta}{h}\tanh\left(\frac{h}{2\delta}\right). \tag{7.8}$$

The normalized distribution of pressure $f'(y_2)$ and motion $f(y_2)$ are shown in Fig. 3 for low, intermediate and high frequencies. Note that the pressure and motions are of weak amplitude and in phase quadrature (real parts are almost zero) at low frequencies. At intermediate frequencies, the fields become complex and non-homogenous Finally, at high frequency the fields are almost real and homogeneous except within the boundary layer on the interface.

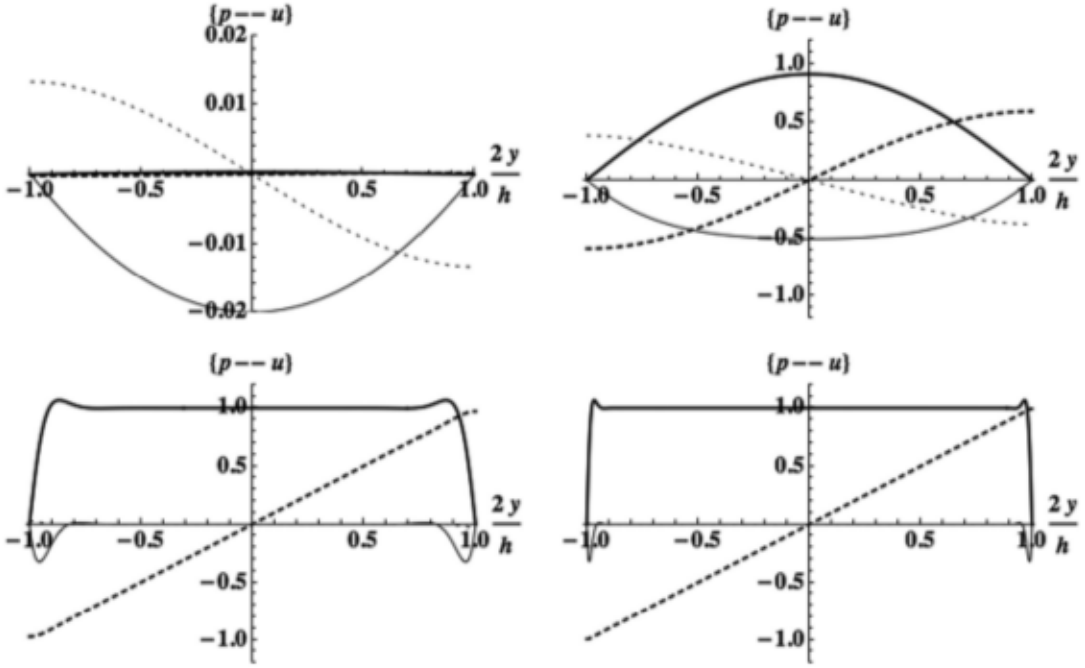

Figure 3. Normalized distributions within the microporous layer, of pressure $f'(y_2)$ (continuous line), and of motion $f(y_2)$ (dashed lines); Real parts are in thick lines, while imaginary parts are in thin lines. The distributions are displayed for low frequency $\omega/\omega_{dp} = 0.02$ (top left), intermediate frequency $\omega/\omega_{dp} = 2$ (top right) and high frequencies $\omega/\omega_{dp} = 20$ (bottom left), $\omega/\omega_{dp} = 200$ (bottom right).

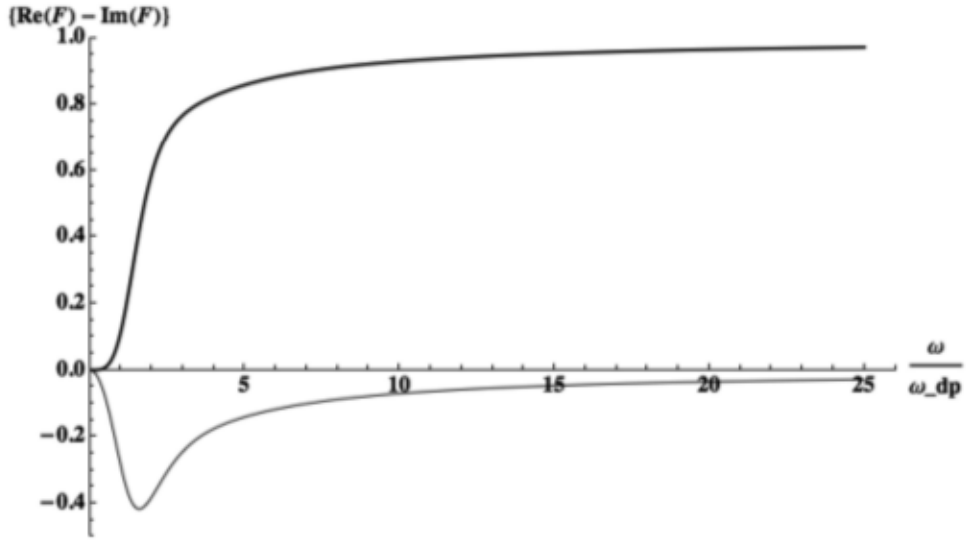

Figure 4. Normalized viscoelastic part F of the effective parameters versus dimensionless frequency $\frac{\omega}{\omega_{dp}}$. Tick line: real part; thin line: imaginary part.

The knowledge of the local fields enables the determination of frequency-dependent parameters (see Appendix A4):

$$\left.\begin{aligned} \widetilde{\mathbf{C}}|_{11}^{11} = \widetilde{\mathbf{C}}_0|_{33}^{11} = (1-\phi_p)\alpha^2 B\left(\frac{2\mu}{\lambda+2\mu}\right)^2 F(\omega); \quad \widetilde{\mathbf{C}}|_{22}^{11} = \widetilde{\mathbf{C}}_0|_{13}^{13} = 0 \\ \widetilde{\mathbf{A}}|_{11} = \widetilde{\mathbf{A}}|_{33} = -(1-\phi_p)\alpha B\frac{2\mu}{\lambda+2\mu}\left(\alpha\frac{\alpha-1}{\lambda+2\mu}+\frac{1}{M}\right)F(\omega); \quad \widetilde{\mathbf{A}}|_{22} = 0 \\ \widetilde{\mathcal{M}}^{-1}(\omega) = -(1-\phi_p)B\left(\alpha\frac{\alpha-1}{\lambda+2\mu}+\frac{1}{M}\right)^2 F(\omega) \end{aligned}\right\} \tag{7.9}$$

The frequency dependence of the kernel function $F(\omega)$ is plotted on Fig. 4. The low- and high-frequency variations of $F(\omega)$ simply read:

$$\left.\begin{aligned} F(\omega) \approx \frac{1}{3}\left(\frac{h}{2\delta}\right)^2 = \frac{i\omega\eta h^2}{12\mathrm{K}B} = \frac{i\omega}{\omega_{dp}} \qquad \text{when} \qquad \omega \to 0 \\ F(\omega) \approx 1 - \frac{2\delta}{h} = 1 - \frac{2}{h}\sqrt{\frac{\mathrm{K}B}{i\omega\eta}} = 1 - \mathbb{F}\sqrt{\frac{\omega_{dp}}{i\omega}} \qquad \text{when} \qquad \omega \to \infty \end{aligned}\right\} \tag{7.10}$$

where $\omega_{dp} = (12\mathrm{K}B)/(\eta h^2)$ and $\mathbb{F} = 1/\sqrt{3}$ are the characteristic frequency and the form factor of the stratified double porosity medium, respectively.

Tensors $\widetilde{\mathbf{C}}$ and $\widetilde{\mathbf{A}}$ vanish at zero frequency and tend to real values at high frequency. Furthermore, simple algebra enables to verify that $\mathbf{C}_\infty|_{11}^{11} = \mathbf{C}_0|_{11}^{11} + \widetilde{\mathbf{C}}|_{11}^{11}(\omega \to \infty)$ and similar equalities for the components of $\mathbf{A}$ and for $\mathcal{M}^{-1}$can be found. Again, the response under macroscopic shear is pressure independent, and therefore frequency independent. Consequently, the retardation effects arise only in response to variations of volumetric strain and pore pressure. Furthermore, all the frequency dependent parameters present the same frequency variation as $F(\omega)$.

7.3 Relaxation phenomenon

Relaxation functions are the time history of the effort in response to a Heaviside loading, for example, a homogeneous macroscopic extension, $U_{1,x1}(t) = E_{11}(t) = H(t)$, or a homogeneous pore pressure $P(t) = H(t)$. Consider, for instance, a uniform jump of deformation without pressure change, *i.e*, $E_{11} = H(t)$ and $P(t) = 0$. Then, the normal effective stress and the uniform volume injection required by the mass balance reads:

$$\left.\begin{aligned} S_{11}(t) = \mathbf{C}_0|_{11}^{11} H(t) + \left(\mathbf{C}_\infty|_{11}^{11} - \mathbf{C}_0|_{11}^{11}\right)\widehat{F}(t) \\ \mathcal{V}(t) = \mathbf{A}_0|_{11} H(t) + (\mathbf{A}_\infty|_{11} - \mathbf{A}_0|_{11})\widehat{F}(t) \end{aligned}\right\} \tag{7.11}$$

where:

$$\widehat{F}(t) = \int_{-\infty}^{\infty} \exp(-i\omega t)\frac{F(\omega)}{i\omega}\mathrm{d}\omega. \tag{7.12}$$

Using the residue method for inversion, the relaxation function $\widehat{F}(t)$ is given by:

$$\widehat{F}(t) = \sum_{1}^{\infty} \frac{8}{\pi^2} \frac{\exp\left(-\frac{t}{\tau(2n-1)^2}\right)}{(2n-1)^2}; \qquad \tau = \frac{h^2\eta}{(4\pi)^2 \mathrm{K}B}. \tag{7.13}$$

The characteristic time of decay that arises from the mechanism of consolidation in the microporous domain is of order $O(\tau)$ (see Fig. 5), and is directly related to the permeability of the microporous domain, the bulk compressibility and the size of the layer.

8 DYNAMICS OF DOUBLE POROSITY MEDIA

In order to focus on double porosity effects, we have neglected the inertial terms while establishing the poroelastic double porosity model in Section 4. The extension to dynamics can be performed by simply adding inertial terms as in Auriault & Boutin (1994), provided that the condition of scale separation is still satisfied. The local description in dynamics is then written as follows.

(1) in the microporous medium

$$\left.\begin{aligned} \underline{\mathrm{div}}(\boldsymbol{\Sigma}) &= (1-\phi)\rho_s \underline{\ddot{u}} + \phi\rho_f \underline{\dot{v}}_f \\ \boldsymbol{\Sigma} &= \mathbf{c} : \mathbf{e}(\underline{u}) - \boldsymbol{\alpha} p \underline{\underline{\mathrm{I}}} \\ \mathrm{div}(\underline{q}) &= -\boldsymbol{\alpha} : \mathbf{e}(\dot{\underline{u}}) - \frac{\dot{p}}{M} \\ \underline{q} = \phi(\underline{v}_f - \dot{\underline{u}}) &= -\frac{\mathcal{K}(\omega)}{\eta}.[\underline{\mathrm{grad}}(p) + \rho_f \ddot{\underline{u}}] \end{aligned}\right\} \tag{8.1}$$

where ρ_s and ρ_f are the density of the solid and the fluid, respectively, and where $\mathcal{K}(\omega)$ represents the dynamic permeability which accounts for both viscous and inertial effects on the flow in the micropores.

(2) in the pores

$$\left.\begin{aligned} \underline{\mathrm{div}}(\boldsymbol{\sigma}_p) &= \rho_f \underline{\dot{v}}_p \\ \boldsymbol{\sigma}_p &= -p_p \mathbf{I} + 2\eta \mathbf{D}(\underline{v}_p) \\ \mathrm{div}(\underline{v}_p) &= -\frac{\dot{p}_p}{K_f} \end{aligned}\right\} \tag{8.2}$$

The boundary conditions between both domains remain unchanged and described by eq. (3.3), and the rescaled asymptotic expansions (3.8) and eq. (3.9) still apply. As the inertial terms are of zero order, the homogenization process is almost unchanged (*cf.* Appendix A6). The main differences are the following:

(1) since the pore flow involves inertia, it is now governed by a dynamic Darcy's law, characterized by the dynamic permeability $\mathcal{K}_p(\omega)$;
(2) the local problem in the microporous domain is formally identical to (4.2) except that the real intrinsic permeability K is replaced by the complex dynamic permeability $\mathcal{K}(\omega)$;
(3) the mean inertial terms appear in the macroscopic balance equations.

As a consequence, the dynamics of double porosity media is described by the following set of equations:

$$\left.\begin{aligned} \underline{\mathrm{div}}(\mathbf{S}) + \underline{\mathcal{F}} &= -\omega^2(1-\phi_p)[(1-\phi)\rho_s + \phi\rho_f]\underline{U} + i\omega\phi_p\rho_f \underline{V}_p \\ \mathbf{S} &= \mathbb{C}(\omega,\mathcal{K}) : \mathbf{e}(\underline{U}) - \mathbb{A}(\omega,\mathcal{K}) P_p \underline{\underline{\mathrm{I}}} \\ \phi_p \mathrm{div}(\underline{V}_p - i\omega\underline{U}) + i\omega\mathcal{V} &= i\omega\left(-\mathbb{A}(\omega,\mathcal{K}) : \mathbf{e}(\underline{U}) - \frac{P_p}{\mathbb{M}(\omega,\mathcal{K})}\right) \\ \phi_p(\underline{V}_p - i\omega\underline{U}) &= -\frac{\mathcal{K}_p}{\eta}.[\underline{\mathrm{grad}}(P_p) - \omega^2\rho_f \underline{U}] \end{aligned}\right\} \tag{8.3}$$

The effective tensors $\mathbb{C}(\omega,\mathcal{K})$, $\mathbb{A}(\omega,\mathcal{K})$, $\mathbb{M}(\omega,\mathcal{K})$ are determined exactly in the same manner as for $\mathbf{C}(\omega)$, $\mathbf{A}(\omega)$, $\mathcal{M}(\omega)$, except that K becomes $\mathcal{K}(\omega)$. Therefore, the symmetry properties can be established as in the quasi-static case. Note that, strictly speaking, these tensors are of elasto-visco-inertial nature.

In practice, due to the weak permeability of the micro-porous domain, in most cases the flow regime in the microporous domain remains driven by viscosity, while the flow in the pores may be significantly affected by the inertia. Indeed, the characteristic frequencies characterizing the ratio of viscous to inertial terms in the pore and in the micropore network are:

$$\omega_{cp} = \frac{\eta\phi_p}{|\mathbf{K}_p|\rho_f} \qquad \omega_c = \frac{\eta\phi}{|\mathbf{K}|\rho_f} \quad \text{thus} \quad \omega_{cp}/\omega_c = \frac{|\mathbf{K}|\phi_p}{|\mathbf{K}_p|\phi} \ll 1.$$

Table 1. Usual parameters for porous fractured rocks.

ϕ	ϕ_p	ρ_s (kg m^{-3})	ρ_f (kg m^{-3})	K_s (Pa)	K_f (Pa)
0.2	0.02	2.7×10^3	10^3	7×10^{10}	2×10^9
λ (Pa)	μ (Pa)	α	M (Pa)	K (m^2)	K_p (m^2)
5×10^{10}	6.6×10^{10}	0.86	9.1×10^{10}	1.2×10^{-12}	2×10^{-11}

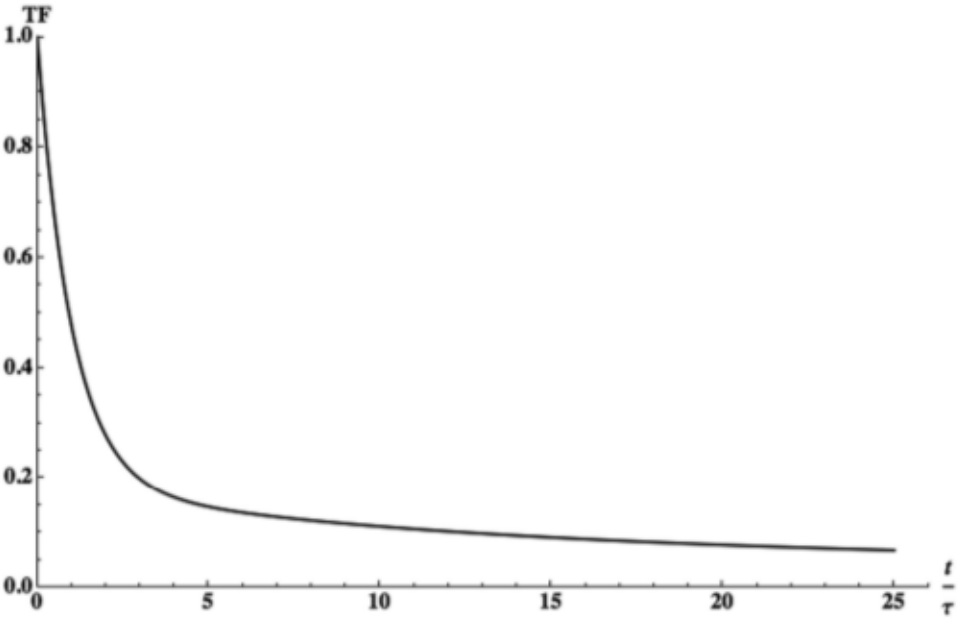

Figure 5. Relaxation function $\widehat{F}(t)$ versus dimensionless time t/τ.

Consequently, in the dynamic description (8.3), $\mathcal{K}_p$ may take complex values (when $\omega > \omega_{cp}$) while $\mathcal{K}$ presents a weak imaginary part (as $\omega_{cp} < \omega < \omega_c$) so that, practically $\mathcal{K} \approx \mathbf{K}$. Hence, as first approximation (of increasing accuracy as ω is lower than ω_c), the tensors $\mathbb{C}(\omega, \mathcal{K})$, $\mathbb{A}(\omega, \mathcal{K})$ and $\mathbb{M}(\omega, \mathcal{K})$ can be replaced by $\mathbf{C}(\omega)$, $\mathbf{A}(\omega)$ and $\mathcal{M}(\omega)$, in the description (8.3). This situation leads to a description similar to a dynamic Biot's model characterized by the dynamic permeability of the pore network $\mathcal{K}_p$ and made of viscoelastic constituents, whose effective tensors are identical to those established in the quasi-static development.

In this context, the features of the complex wave celerity $C(\omega)$ of the P1 compression wave in isotropic double porosity media has been calculated. The derivation of the wave celerity $Re(C(\omega))$ and attenuation $Im(C(\omega))/Re(C(\omega))$ is performed by following the same steps as in a single porosity Biot porous medium (Deresiewickz 1960) and is not detailed here. Calculations have been done with the data displayed on Table 1, which correspond to usual properties of fractured sandstone or limestone oil reservoirs. The frequency range of calculation is limited to $\omega = 750$ Hz so that the inertial flow effect is negligible. Hence, intrinsic permeabilities have been used. For simplicity, we use the frequency-dependent viscoelastic function (7.8) deduced for the stratified case. Figs 6 and 7 show wave dispersion and attenuation in two distinct fractured porous rocks made of the same porous matrix with fracture spacing of $h = 4m$ and $h = 2.3m$, respectively, corresponding to characteristic frequencies ω_{dp} of 100 Hz and 300 Hz, respectively. The comparison with the values for the (single-porosity) porous matrix highlights the double porosity effect:

(1) Double porosity enhances the dispersion of the P1 wave. However, this perturbation is of the order of 1 per cent and can be neglected in practice.

(2) Double porosity enhances the attenuation of the P1 wave of a factor of about 3 in a frequency range associated to the characteristic double porosity frequency. Note further that, conversely to the P1 attenuation in the single porosity Biot model, here the attenuation is not proportional to the frequency. This difference is a consequence of the significant fluid/solid relative motions which are induced inside the microporous domain and which give rise energy dissipation by viscous effect. Conversely, in a single porosity medium, the fluid and solid motions are almost identical under the propagation of a P1 wave and the dissipation is smaller. This additional attenuation is a possible explanation of the observed attenuation of seismic waves which cannot be adequately accounted for by the classic Biot model.

For more general applications of the theory to practical cases a numerical implementation is required. In the frequency domain this task should be relatively easy by introducing the complex effective parameters. In the time domain much efforts are necessary to address the induced memory effects. A comprehensive analysis of these complex numerical aspects is a specific topic itself, which is out of the scope of this paper.

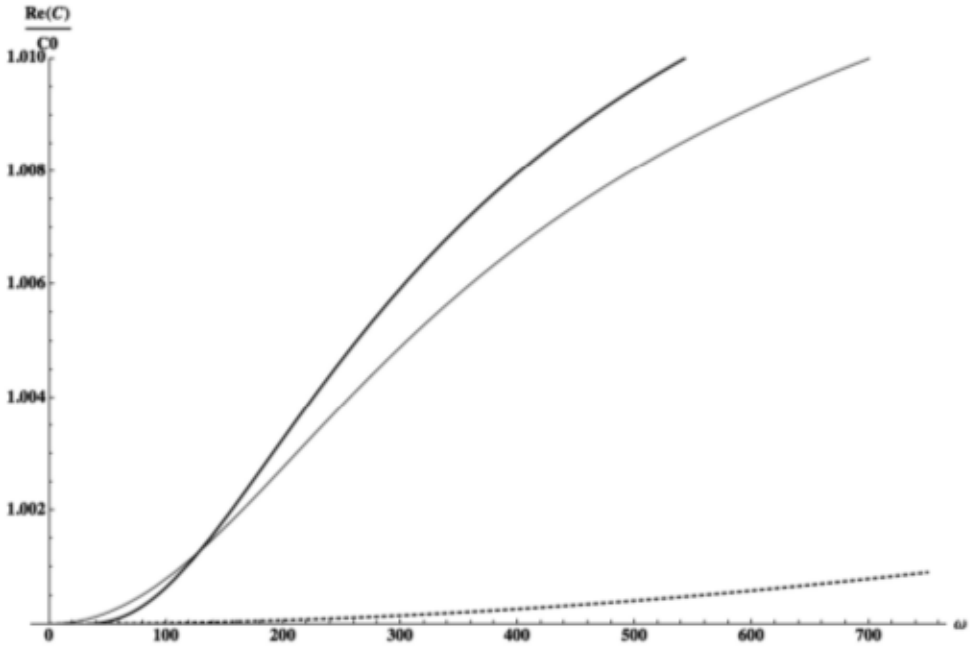

Figure 6. Dispersion of the P1 wave velocity $Re(C(\omega))/C(0)$ of two fractured porous rocks characterized by $\omega_{db} = 100$ Hz (thick line); 300 Hz (normal line). The dispersion corresponding to the constitutive (single porosity) porous matrix is given for comparison (dashed line). The reference celerity deduced from values of Table 1, is $C(0) = 2.66 \times 10^3$ m s^{-1}.

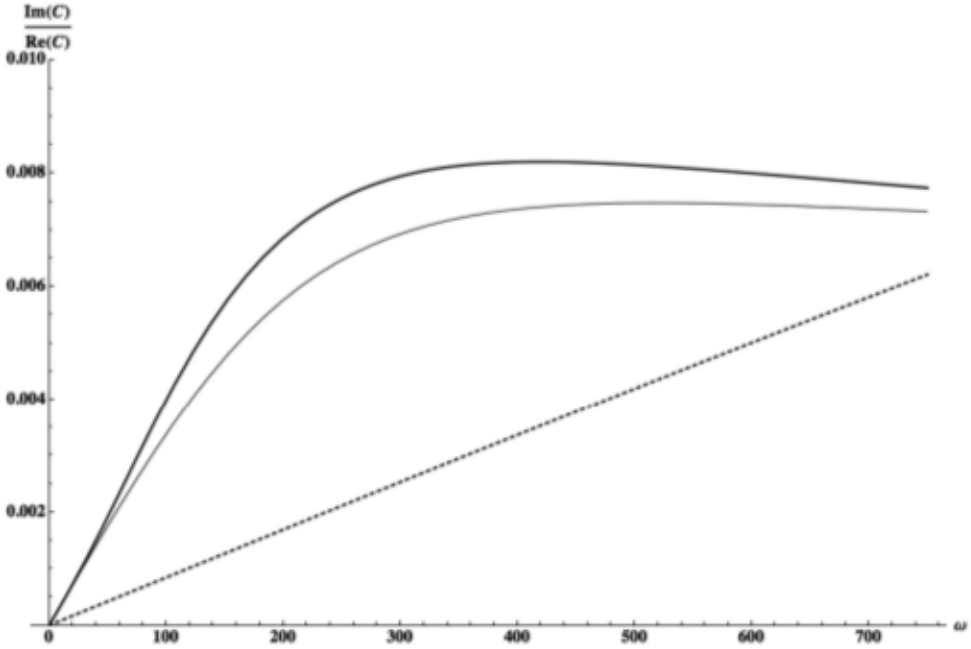

Figure 7. P1 wave attenuation $Im(C(\omega))/Re(C(\omega))$ of two fractured porous rocks characterized by $\omega_{db} = 100$ Hz (thick line); 300 Hz (normal line). The attenuation corresponding to the constitutive (single porosity) porous matrix is given for comparison (dashed line).

9 CONCLUSION

This work presents the links between between (i) the micro/meso morphology and (ii) the timescale of evolution and the corresponding structure of the model for double porosity poroelastic media.

The dual-porosity macroscopic behaviour, that is, the two-pressure-field macroscopic behaviour is obtained by homogenization when the characteristic time of consolidation in the microporous domain is of same order as the macroscopic characteristic time of the transient regime. This corresponds to a permeability ratio $K/K_p = \varepsilon^2 \ll 1$. The coupling tensors of the dual-porosity poroelastic model are shown to be equal, which proves the symmetrical coupling between pressure and solid deformation. Consequently, the macroscopic model is similar to the classical biphasic Biot model, but with complex-valued and frequency-dependent effective stiffness, coupling tensor and compressibility, that correspond to apparent viscoelastic properties of the solid and the fluid. In transient regime, these viscoelastic effects lead to retardation

Table 2. The relevant behaviours and their effective parameters according to the frequency ω compared to the three characteristic frequencies of the micropore diffusion process ω_{dp}, and the flow regime in the pores ω_{cp}, and in micropores ω_c. Top: Quasi-static case model (4.12), Bottom: Dynamic model (8.3).

Quasi-static Model (4.12) ; $\omega_{dp} \ll \omega_{cp}$			
$\omega \ll \omega_{dp}$	$\omega = O(\omega_{dp})$	$\omega_{dp} \ll \omega < \omega_{cp}$	$\omega_{cp} < \omega < \omega_c$
Single porosity	**Double porosity**	**Single porosity**	
Drained micropores	Transient regime	Undrained micropores	
$\mathbf{C}_0$, $\mathbf{A}_0$, $\mathcal{M}_0$	$\mathbf{C}(\omega)$, $\mathbf{A}(\omega)$, $\mathcal{M}(\omega)$	$\mathbf{C}_\infty$, $\mathbf{A}_\infty$, $\mathcal{M}_\infty$	
Viscous regime of pore and micropore flow			Dynamic pore flow
$\mathbf{K}_p$			$\mathcal{K}_p(\omega)$

Dynamic Model (8.3) ; $\omega_{dp} = O(\omega_{cp}) < \omega_c$		
$\omega \ll \omega_{dp}$	$\omega = O(\omega_{dp}) = O(\omega_{cp})$	$\omega_{dp} \ll \omega$
Single porosity	**Double porosity**	**Single porosity**
Drained micropores	Transient regime	Undrained micropores
$\mathbf{C}_0$, $\mathbf{A}_0$, $\mathcal{M}_0$	$\mathbb{C}(\omega, \mathcal{K})$, $\mathbb{A}(\omega, \mathcal{K})$, $\mathbb{M}(\omega, \mathcal{K})$	$\mathbf{C}_\infty$, $\mathbf{A}_\infty$, $\mathcal{M}_\infty$
Viscous flow in pores (and micropores)	Dynamic regime of pore (and micropore) flow	
$\mathbf{K}_p$; (**K**)	$\mathcal{K}_p(\omega)$; ($\mathcal{K}(\omega)$)	

effects expressed in terms of convolution products. It is also shown how the use of a spectral decomposition allows to take into account the apparent viscoelastic effects without introducing convolution products, which is more convenient for computational issues. When considering a higher permeability contrast $K/K_p \leq \varepsilon^3$, the corresponding description is the high-frequency limit of the above mentioned double porosity model. Conversely, a weaker contrast $K/K_p \geq \varepsilon$ leads to the quasi-static description. This shows that the permeability scaling is in fact strongly related to the regime experienced by the microporous domain. This regime is characterized by the ratio between the characteristic time of consolidation in the microporous matrix τ and the characteristic macroscopic time of the phenomenon T:

(1) if $T/\tau = O(1)$: the double porosity model with memory (or viscoelactic) effects applies. Both the microporous and the macroscopic domains experience a transient regime and two distinct pressure fields coexist.

(2) if $T/\tau \gg O(1)$: the low-frequency limit of the double porosity model applies. The pore and the macropore domains undergo the same pressure, and the description is the usual Biot's one.

(3) if $T/\tau \ll O(1)$: the high-frequency limit of the double porosity model applies. The medium is described by a Biot model whose effective elastic tensor takes into account the fact that the microporous domain is saturated by a static fluid.

In other words, the double porosity behaviour is reached when a transient consolidation process arises within the microporous domain. Conversely, for long (respectively short) time evolution the microporous domain behaves in drained (respectively undrained) conditions, and usual Biot descriptions applies (with different effective parameters). The frequency range of validity of different behaviours are shown in Table 2.

The time-dependent interaction between both porous networks is an essential feature of the behaviour of double porosity media with contrasted permeability. Conversely, an instantaneous interaction is assumed in the phenomenological models extending the BZK or WR models to deformable solids. We have shown that the instantaneous assumption does not describe a double porosity microstructure but a medium with two pore networks of contrasted permeabilities, separated by a thin layer of much smaller permeability which constitutes an interface flow barrier. In practice, this specific morphology is less usual than the actual double porosity one. Furthermore, these models fail at predicting and reproducing the behaviour of usual double porosity media.

These results are of particular interest in reservoir geophysics, ultrasonic and seismic exploration. Indeed, the models enable to characterize the seismic response of geologic formations. For instance, the frequency spectra of the loss mechanisms occurring in single porosity, double porosity or media with interface flow barrier are of different natures. The model introduced in this paper provides an interpreting tool for identifying the actual morphology of complex saturated porous media.

In dynamic regime, the results are very similar to those derived in quasi-static regime, provided that the scale separation requirement is satisfied. It is worth reminding that the results established in this paper for periodic materials with separated scales formally apply to non-periodic materials for which a REV can be defined (Auriault *et al.* 2009). Note however, that the determination of the effective parameters is then not reducible to a well-defined problem to be solved in a periodic cell. Finally, the models can also be extended to patchy porous media with highly contrasted permeabilities.

ACKNOWLEDGEMENTS

The authors gratefully acknowledge Dr Rodolfo Venegas for his fruitful comments that greatly improved the manuscript.

REFERENCES

Arbogast, T., 1989. Analysis of the simulation of single-phase flow through a naturally fractured reservoir, *SIAM J. Numer. Anal.*, **26,** 12–29.

Arbogast, T., 1997. Computational aspects of dual-porosity models, in *Homogenization and Porous Media,* pp. 203–223, ed. Hornung, U., Springer.

Arbogast, T., Douglas, J. & Hornung, U., 1990. Derivation of the double porosity model of single phase flow via homogenization theory, *SIAM J. Math. Anal.*, **21**(4), 823–836.

Auriault, J.L., 1980. Dynamic behavior of a porous medium saturated by a Newtonian fluid, *Int. J. Eng. Sci.*, **18,** 775–785.

Auriault, J.-L., 1983. Effective macroscopic description for heat conduction in periodic composites, *Int. J. Heat Mass Transfer,* **26**(6), 861–869.

Auriault, J.-L., 1991. Heterogeneous medium. Is an equivalent macroscopic description possible?, *Int. J. Eng. Sci.*, **29**(7), 785–795.

Auriault, J.-L. & Boutin, C., 1992. Deformable porous media with double porosity. Quasi-statics. I. Coupling effects, *Transp. Porous Media,* **7,** 63–82.

Auriault, J.-L. & Boutin, C., 1993. Deformable porous media with double porosity. Quasi-statics. II. Memory effects, *Transp. Porous Media,* **10,** 153–169.

Auriault, J.-L. & Boutin, C., 1994. Deformable porous media with double porosity. III. Acoustics, *Transp. Porous Media,* **14,** 143–162.

Auriault, J.-L. & Ene, H.I., 1994. Macroscopic modelling of heat transfer in composites with interfacial thermal barriers, *Int. J. Heat Mass Transfer,* **38**(18), 2885–2892.

Auriault, J.-L. & Lewandowska, J., 1995. Non-Gaussian diffusion modeling in composite porous media by homogenization: tail effect, *Transp. Porous Media,* **21,** 47–70.

Auriault, J.-L. & Royer, P., 1993. Double conductivity media: a comparison between phenomenological and homogenization approaches, *Int. J. Heat Mass Transfer,* **36**(10), 2613–2621.

Auriault, J.-L. & Sanchez-Palencia, E., 1977. Etude du comportement macroscopique d'un milieu poreux saturé déformable, *J. Mec.*, **16,** 37–53.

Auriault, J.-L., Boutin, C. & Geindreau, C., 2009. *Homogenization of Coupled Phenomena in Heterogeneous Media,* Wiley-ISTE.

Bai, M., Elsworth, D. & Roegiers, J.-C., 1993. Modeling of naturally fractured reservoirs using deformation dependent flow mechanism, *Int. J. Rock Mech. Min. Sci. Geomech. Abstr.*, **30,** 1185–1191.

Barenblatt, G.I., 1963. On certain boundary-value-problems for the equations of seepage of liquid in fissured rocks, *PMM,* **27**(2), 348–350.

Barenblatt, G.I. & Zheltov Iu. & Kochina, I.N., 1960. Basic concept in the theory of seepage of homogeneous liquids in fissured rocks, *Prikl. Mat. Mekh.*, **24**(5), 852–864 (in Russian); *J. Appl. Math. Mech.*, **24,** 1286–1303.

Berryman, J.G. & Wang, F.W., 1995. The elastic coefficients of double-porosity models for fluid transport in jointed rock, *J. geophys. Res.*, **100**(B12), 24 611–24 627.

Beskos, D.E. & Aifantis, E.C., 1986. On the theory of consolidation with double porosity, II, *Int. J. Engng. Sci.*, **24,** 1697–1716.

Biot, M.A., 1956a. Theory of propagation of elastic waves in a fluid-saturated porous solid. I. Low-frequency gange, *J. acoust. Soc. Am.*, **28,** 168–178.

Biot, M.A., 1956b. Theory of propagation of elastic waves in a fluid-saturated porous solid. II. Higher frequency range, *J. acoust. Soc. Am.*, **28,** 179–191.

Boutin, C. & Auriault, J.-L., 1990. Dynamic behavior of porous media saturated by a viscoelastic fluid. Application to bituminous concretes, *Int. J. Eng. Sci.*, **11,** 1157–1181.

Boutin, C., Royer, P. & Auriault, J.-L., 1998. Acoustic absorption of porous surfacing with dual porosity, *Int. J. Solids Struct.*, **35,** 4709–4737.

Brajanovski, M., Müller, T.M. & Gurevich, B., 2006. Characteristic frequencies of seismic attenuation due to wave-induced fluid flow in fractured porous media, *Geophys. J. Int.*, **166**(2), 574–578.

Carcione, J.M., Morency, C. & Santos, J.E., 2010. Computational poroelasticity - A review *Geophysics,* **75**(5), 75A229–75A243.

Courant, R. & Hilbert, D., 1970. *Methods of Mathematical Physics,* Vol. 1, 8th edn, 561p, Interscience Publishers Inc.

dell'Isola, F., Rosa, L. & Wozniak, C., 1997a. Micro-structured continuum modelling compacting fluid-saturated grounds: the effects of Poze-size scale parameter, *Acta Mech.*, **127,** 165–182.

dell'Isola, F., Rosa, L. & Wozniak, C., 1997b. Dynamics of solids with microperiodic nonconnected fluid inclusions, *Arch. Appl. Mech.*, **67**(4), 215–228.

Deresiewickz, H., 1960. The effect of boundaries on wave propagation in a liquid filled porous solid. I, *Bull. seism. Soc. Am.*, **50,** 597–607.

Eringen, A.C., 1968. Mechanics of micromorphic continua, in *IUTAM Symposium,* pp. 18–35, ed. Kröner, E., Springer-Verlag.

Grechka, V., Mazumdar, P. & Shapiro, S.A., 2010. Predicting permeability and gas production of hydraulically fractured tight sands from microseismic data, *Geophysics,* **75**(1), B1–B10.

Hornung, U. & Showalter, R.R., 1990. Diffusion models for fractured media, *J. Math. Anal. Appl.*, **147,** 69–80.

Lewandowska, J., Tran Ngoc, T.D., Vauclin, M. & Bertin, H., 2008. Water drainage in double-porosity soils: experiments and micro-macro modeling, *J. Geotech. Geoenviron. Eng.*, **134**(2), 231–243.

Liu, X., Greenhalgh, S.A. & Zhou, B., 2009. Transient Solution for poro-viscoacoustic wave propagation in double porosity media, and its Limitations, *Geophys. J. Int.*, **178,** 375–393.

Müller, T.M., Gurevich, B. & Lebedev, M., 2010. Seismic wave attenuation and dispersion resulting from wave-induced flow in porous rocks—a review, *Geophysics,* **75**(5), 75A147–75A164.

Murad, M.A., Guerreiro, J.N. & Loula, A.F.D., 2001. Micromechanical computational modelling of secondary consolidation and hereditary creep in soils, *Comput. Methods Appl. Mech. Eng.*, **190,** 1985–2016.

Ngoc, T.D., Lewandowska, J. & Bertin, H., 2007. Etude expérimentale d'un milieu à double porosité en conditions saturée et insaturée, *18éme Cong. Franç. Mec. - Grenoble,* 6p.

Olny, X., 1999. Absorption acoustique des milieux poreux à simple et double porosité. Modélisation et validation expérimentale, *PhD ENTPE/INSA,* 280p.

Olny, X. & Boutin, C., 2003. Acoustic wave propagation in double porosity media, *J. acoust. Soc. Am.*, **113**(6), 73–89.

Parotidis, M., Rothert, E. & Shapiro, S.A., 2003. Pore-pressure diffusion: A possible triggering mechanism for the earthquake swarms 2000 in Vogtland/NW/Bohemia, Central Europe, *Geophys. Res. Lett.*, **30**(20), doi:10.1029/2003GL018110.

Pride, S., 2005. Relationships between seismic and hydrological properties, in *Hydrogeophysics, Water Science and Technology Library,* Springer, pp. 253–284.

Pride, S.R. & Berryman, J.G., 2003. Linear dynamics of double-porosity dual-permeability materials. II. Fluid transport equations, *Physical Review E,* **68**(3), doi:10.1103/PhysRevE.68.036604.

Royer, P. & Auriault, J.-L., 1994. Transient quasi-static gas flow through a rigid porous medium with double porosity, *Transp. Porous Media,* **17,** 33–57.

Royer, P. & Auriault, J.L., 1999. Homogenization of compressible fluid flow in porous media with interfacial flow barrier, *Arch. Mech.*, **51**(3–4), 469–486.

Royer, P. & Boutin, C., 2012. Time analysis of the three characteristic behaviors of dual-porosity media. I. Fluid flow and solute transport, *Transp. Porous Media,* **95,** 603–626.

Royer, P., Auriault, J.-L. & Boutin, C., 1996. Macroscopic modeling of double-porosity reservoirs, *J. Pet. Sci. Eng.*, **16,** 187–202.

Sanchez-Palencia, E., 1980. *Non-Homogeneous Media and Vibration Theory,* Lecture Notes in Physics 127, Springer-Verlag.

Shapiro, S.A., 2000. An inversion for fluid transport properties of three dimensionally heterogeneous rocks using induced microseismicity, *Geophys. J. Int.*, **143**(3), 931–936.

Venegas, R. & Umnova, O., 2011. Acoustic properties of double porosity granumar materials, *J. acoust. Soc. Am.*, **130**(5), 2765–2776.

Warren, J.E. & Root, P.J., 1963. The behavior of naturally fractured reservoirs. *J. Soc. Pet. Eng.*, **3,** 245–255.

Wilson, R.K. & Aifantis, E.C., 1982. On the theory of consolidation with double porosity, *Int. J. Eng. Sci.*, **20**(9), 1009–1035.

Wilson, R.K. & Aifantis, E.C., 1984. A double porosity model for acoustic wave propagation in fractured-porous rock, *Int. J. Eng. Sci.*, **22**(8–10), 1209–1217.

APPENDIX A: HOMOGENIZATION PROCESS

Introducing the asymptotic expansions into the set of governing equations, while taking into account estimates presented in Section 3.5, we get the following boundary value problems of successive orders of magnitude of ε.

A1 Leading order problems in Ω and Ω_p

In the microporous domain, the leading order problem simply reads:

$$\left.\begin{aligned} \underline{\mathrm{div}}_y\left(\mathbf{c} : \mathbf{e}_y(\underline{u}^0)\right) &= \underline{0} \qquad \text{in } \Omega \\ \left(\mathbf{c} : \mathbf{e}_y(\underline{u}^0)\right).\underline{n} &= \underline{0} \qquad \text{on } \Gamma \\ \underline{u}^0, \quad \widehat{\Omega} &- \text{periodic} \end{aligned}\right\} \tag{A1}$$

This is a classical local problem for an elastic porous skeleton whose solution is (Auriault 1980) :

$$\underline{u}^0(\underline{x}, \underline{y}) = \underline{U}(\underline{x}) \tag{A2}$$

For the pores at the leading order we have $\underline{\mathrm{div}}_y(-p_p^0\mathbf{I}) = -\underline{\mathrm{grad}}_y(p_p^0) = \underline{0}$, thus

$$p_p^0(\underline{x}, \underline{y}) = P_p(\underline{x}). \tag{A3}$$

A2 Local problem in the pore domain Ω_p

In the pores, the second-order problem reads:

$$\left.\begin{aligned} -\underline{\mathrm{grad}}_y(p_p^1) - \underline{\mathrm{grad}}_x(P_p) + \eta\underline{\Delta}_y(\underline{v}_p^0) &= \underline{0} \qquad \text{in } \Omega_p \\ \mathrm{div}(\underline{v}_p^0) &= 0 \qquad \text{in } \Omega_p \\ \underline{v}_p^0 - i\omega\underline{U} &= 0 \qquad \text{on } \Gamma \end{aligned}\right\}$$

This is the well-known local problem defining the Darcy's law, from which we obtain:

$$\underline{v}_p^0 - i\omega\underline{U} = -\frac{\mathbf{k}_p}{\eta}.\underline{\mathrm{grad}}_x(P_p).$$

The particular solutions $\underline{k}_p^j$ corresponding to $\mathrm{grad}_{xj}(P_p) = \delta_{ij}$ (δ is the Kronecker symbol) are real valued. Defining the mean fluid motion in the pores and the tensor of intrinsic permeability respectively by

$$\underline{V}_p = \frac{1}{\Omega_p}\int_{\Omega_p} \underline{v}_p^0 \, \mathrm{d}\Omega; \qquad \mathbf{K}_p = \frac{1}{\Omega_p}\int_{\Omega_p} \mathbf{k}_p \, \mathrm{d}\Omega \tag{A4}$$

we get the usual Darcy's law :

$$\phi_p(\underline{V}_p - i\omega\underline{U}) = -\frac{\mathbf{K}_p}{\eta}.\underline{\mathrm{grad}}_x(P_p). \tag{A5}$$

A3 Next order local problem in the microporous domain Ω

The first order problem in Ω is given by the set of equations (4.2). Note that, as expected, this frequency-dependent problem is the one obtained using the three scale approach in Auriault & Boutin (1993). Before investigating the solution at any frequency, let us consider the long- and short-term responses reached at zero and 'infinite' frequency respectively.

A3.1 Low-frequency (long-term) local response

When $\omega = 0$, eqs (4.2–c,d) lead to the trivial solution $p^0(\omega = 0) = P_p(\underline{x})$. Thus, denoting $\underline{u}^1(\omega = 0) = \underline{u}_0^1$, (4.2–a,b,e) become:

$$\left.\begin{aligned} \underline{\mathrm{div}}_y\left(\mathbf{c} : (\mathbf{e}_x(\underline{U}) + \mathbf{e}_y(\underline{u}_0^1)) - \boldsymbol{\alpha}P_p\right) &= \underline{0} \qquad \text{in } \Omega \\ \left(\mathbf{c} : \left(\mathbf{e}_x(\underline{U}) + \mathbf{e}_y(\underline{u}_0^1)\right) - \boldsymbol{\alpha}\right)P_p\big).\underline{n} &= -P_p\,\underline{n} \qquad \text{on } \Gamma \\ \underline{u}_0^1, \quad \widehat{\Omega} &- \text{periodic} \end{aligned}\right\} \tag{A6}$$

The microporous domain reacts with the skeleton elastic tensor $\mathbf{c}$ to the macroscopic strain $\mathbf{e}_x(\underline{U})$ and pore pressure P_p, both acting as forcing terms. The equivalent variational formulation is derived by taking the scalar product of eq. (A6-a) with a $\widehat{\Omega}$-periodic test field $\underline{w}$ defined over Ω, and then by integrating over Ω. The $\widehat{\Omega}$-periodicity provides:

$$\forall \underline{w}\ \widehat{\Omega}-\text{periodic} \qquad \int_{\partial\Omega\cap\partial\widehat{\Omega}} [\left(\mathbf{c} : (\mathbf{e}_x(\underline{U}) + \mathbf{e}_y(\underline{u}_0^1)) - \boldsymbol{\alpha} P_p\right).\underline{n}].\underline{w}\, ds = 0 \tag{A7}$$

Then, using the divergence theorem, the symmetry of $\mathbf{c}$ and $\boldsymbol{\alpha}$, and boundary condition (A6-b) on Γ and periodicity (A6-c), we obtain:

$$\forall \underline{w}\ \widehat{\Omega}-\text{periodic} \qquad \int_{\Omega} \mathbf{e}_y(\underline{w}) : \mathbf{c} : \mathbf{e}_y(\underline{u}_0^1)\, \mathrm{d}\Omega = -\int_{\Omega} [\mathbf{e}_y(\underline{w}) : \mathbf{c} : \mathbf{e}_x(\underline{U}) + \mathbf{e}_y(\underline{w}) : (\mathbf{I} - \boldsymbol{\alpha}) P_p]\, \mathrm{d}\Omega. \tag{A8}$$

Thus, owing to the ellipticity and symmetry of $\mathbf{c}$, the Lax-Milgram lemma ensures the existence and uniqueness of $\underline{u}_0^1(\underline{x}, \underline{y})$ (modulo a uniform translation field). The local field is real, independent of the frequency and takes the form:

$$\underline{u}_0^1(\underline{x}, \underline{y}) = \boldsymbol{\xi}_0(\underline{y}) : \mathbf{e}_x(\underline{U}) - \zeta_0(\underline{y}) P_p = \underline{\xi}_0^{ij} e_{xij}(\underline{U}) - \underline{\zeta}_0(\underline{y}) P_p. \tag{A9}$$

Solutions $\underline{\xi}_0^{ij}$ and $\underline{\zeta}_0$, of zero mean value on Ω, correspond to $e_{xij}(\underline{U}) = (\delta_{ij} + \delta_{ji})/2$ and $P_p = 1$, respectively.

A3.2 High-frequency (short-term) local response

When $\omega \to \infty$, denoting $p^0(\omega \to \infty) = p_\infty$ and $\underline{u}^1(\omega \to \infty) = \underline{u}_\infty^1$, the mass balance (4.2–c) implies that:

$$p_\infty = -M\boldsymbol{\alpha} : \left(\mathbf{e}_x(\underline{U}) + \mathbf{e}_y(\underline{u}_\infty^1)\right) \tag{A10}$$

Reporting this expression in (14-a,b) provides ($\otimes$ denotes the tensorial product) :

$$\left.\begin{aligned} \mathrm{div}_y\left([\mathbf{c} + M\boldsymbol{\alpha} \otimes \boldsymbol{\alpha}] : (\mathbf{e}_x(\underline{U}) + \mathbf{e}_y(\underline{u}_\infty^1))\right) &= \underline{0} \qquad \text{in } \Omega \\ \left([\mathbf{c} + M\boldsymbol{\alpha} \otimes \boldsymbol{\alpha}] : \left(\mathbf{e}_x(\underline{U}) + \mathbf{e}_y(\underline{u}_\infty^1)\right)\right).\underline{n} &= -P_p \underline{n} \qquad \text{on } \Gamma \\ \underline{u}_\infty^1, \quad \widehat{\Omega} &- \text{periodic} \end{aligned}\right\} \tag{A11}$$

This means that the microporous domain behaves as a medium with elastic tensor $\mathbf{c}_\infty = \mathbf{c} + M\boldsymbol{\alpha} \otimes \boldsymbol{\alpha}$. From the periodicity we have:

$$\forall \underline{w}\ \widehat{\Omega}-\text{periodic} \qquad \int_{\partial\Omega\cap\partial\widehat{\Omega}} [\left(\mathbf{c}_\infty : (\mathbf{e}_x(\underline{U}) + \mathbf{e}_y(\underline{u}_\infty^1)\right).\underline{n}].\underline{w}\, \mathrm{d}s = 0 \tag{A12}$$

and applying the same reasoning as above, the variational formulation reads:

$$\forall \underline{w}\ \widehat{\Omega}-\text{periodic} \qquad \int_{\Omega} \mathbf{e}_y(\underline{w}) : \mathbf{c}_\infty : \mathbf{e}_y(\underline{u}_\infty^1)\, \mathrm{d}\Omega = -\int_{\Omega} [\mathbf{e}_y(\underline{w}) : \mathbf{c}_\infty : \mathbf{e}_x(\underline{U}) + P_p \mathrm{div}_y(\underline{w})]\, \mathrm{d}\Omega\,. \tag{A13}$$

Hence, the local field is real, independent of the frequency and takes the form:

$$\underline{u}_\infty^1(\underline{x}, \underline{y}) = \boldsymbol{\xi}_\infty(\underline{y}) : \mathbf{e}_x(\underline{U}) - \underline{\zeta}_\infty(\underline{y}) P_p = \underline{\xi}_\infty^{ij} e_{xij}(\underline{U}) - \underline{\zeta}_\infty(\underline{y}) P_p \tag{A14}$$

where $\underline{\xi}_\infty^{ij}$ and $\underline{\zeta}_\infty$, are of zero mean value on Ω, and correspond respectively to $e_{xij}(\underline{U}) = (\delta_{ij} + \delta_{ji})/2$ and $P_p = 1$. The pressure can then be written as

$$\left.\begin{aligned} p_\infty(\underline{x}, \underline{y}) = \boldsymbol{\theta}_\infty(\underline{y}) : \mathbf{e}_x(\underline{U}) + (1 - \varpi_\infty(\underline{y})) P_p \\ \boldsymbol{\theta}_\infty = -M\boldsymbol{\alpha} : (\mathbf{e}_y(\boldsymbol{\xi}_\infty) + \mathbf{I}) \\ 1 - \varpi_\infty = M\boldsymbol{\alpha} : \mathbf{e}_y(\underline{\zeta}_\infty) \end{aligned}\right\} \tag{A15}$$

A3.3 Local response at any frequency ω

By virtue of linearity, the solution $(\underline{u}^1, p^0)$ at any frequency can be decomposed into the sum of the long-term solution $(\underline{u}_0, P_p)$ and of the frequency-dependent fields $(\underline{\widetilde{u}}(\omega), \widetilde{p}(\omega))$:

$$\underline{u}^1 = \underline{u}_0^1 + \underline{\widetilde{u}}(\omega); \qquad p^0 = P_p + \widetilde{p}(\omega). \tag{A16}$$

We then deduce that $(\widetilde{\underline{u}}, \widetilde{p})$ is solution to the following set of equations:

$$\left.\begin{aligned} \underline{\mathrm{div}}_y\left(\mathbf{c} : \mathbf{e}_y(\widetilde{\underline{u}}) - \boldsymbol{\alpha}\widetilde{p}\right) &= \underline{0} && \text{in } \Omega \\ \left(\mathbf{c} : \mathbf{e}_y(\widetilde{\underline{u}}) - \boldsymbol{\alpha}\widetilde{p}\right).\underline{n} &= \underline{0} && \text{on } \Gamma \\ \frac{1}{i\omega\eta}\mathrm{div}_y(\mathbf{K}.\underline{\mathrm{grad}}_y(\widetilde{p})) = \boldsymbol{\alpha} : \mathbf{e}_y(\widetilde{\underline{u}}) + \frac{\widetilde{p}}{M} + \boldsymbol{\alpha} : (\mathbf{e}_x(\underline{U}) + \mathbf{e}_y(\underline{u}_0^1)) + \frac{P_p}{M} && \text{in } \Omega \\ \widetilde{p} &= 0 && \text{on } \Gamma \\ \widetilde{\underline{u}} \quad \text{and} \quad \widetilde{p}, \quad \widehat{\Omega} - \text{periodic} \end{aligned}\right\} \tag{A17}$$

To formulate the solution, let us first relate $\widetilde{\underline{u}}$ to $\widetilde{p}$. For this propose, we take the scalar product of eq. (A17-a) with any $\widehat{\Omega}$-periodic field $\underline{w}$ defined on Ω, and then integrate over Ω. From the $\widehat{\Omega}$-periodicity we have:

$$\forall \underline{w}\ \widehat{\Omega} - \text{periodic} \qquad \int_{\partial\Omega\cap\partial\widehat{\Omega}} [\left(\mathbf{c} : \mathbf{e}_y(\widetilde{\underline{u}}) - \boldsymbol{\alpha}\widetilde{p}\right).\underline{n}].\underline{w}\,\mathrm{d}s = 0, \tag{A18}$$

Using the divergence theorem, the symmetries of $\mathbf{c}$ and $\boldsymbol{\alpha}$, and the boundary condition (A17-b) on Γ we derive that:

$$\forall \underline{w}\ \widehat{\Omega} - \text{periodic} \qquad \int_\Omega \mathbf{e}_y(\underline{w}) : \mathbf{c} : \mathbf{e}_y(\widetilde{\underline{u}})\,\mathrm{d}\Omega = \int_\Omega \boldsymbol{\alpha} : \mathbf{e}_y(\underline{w})\widetilde{p}\,\mathrm{d}\Omega. \tag{A19}$$

Thus, owing to the ellipticity and symmetry of $\mathbf{c}$, the Lax-Milgram lemma insures that $\widetilde{\underline{u}}$ exists and is uniquely determined once $\widetilde{p}$ is defined. Consequently, we can write:

$$\widetilde{\underline{u}} = \widetilde{\underline{u}}(\widetilde{p}), \tag{A20}$$

and for any $\widehat{\Omega}$-periodic pressure field π defined on Ω, we have

$$\forall \pi\ \widehat{\Omega} - \text{periodic} \qquad \int_\Omega \mathbf{e}_y(\widetilde{\underline{u}}(\pi)) : \mathbf{c} : \mathbf{e}_y(\widetilde{\underline{u}}(\widetilde{p}))\,\mathrm{d}\Omega = \int_\Omega \boldsymbol{\alpha} : \mathbf{e}_y(\widetilde{\underline{u}}(\pi))\widetilde{p}\,\mathrm{d}\Omega. \tag{A21}$$

We can now look for the resolution. By construction, $\widetilde{p}$ belongs to the space $\mathcal{P}$ of $\widehat{\Omega}$-periodic and complex valued pressure field π defined on Ω, with $\pi = 0$ on Γ. Multiplying (A17-c) by any $\pi \in \mathcal{P}$, integrating over Ω, and considering the $\widehat{\Omega}$-periodicity one can deduce that:

$$\forall \pi \in \mathcal{P} \qquad \frac{1}{i\omega\eta}\int_{\partial\Omega\cap\partial\widehat{\Omega}} \left[\left(\mathbf{K}.\underline{\mathrm{grad}}_y(\widetilde{p})\right).\underline{n}\right].\underline{w}\,\mathrm{d}s = 0. \tag{A22}$$

The divergence theorem, and boundary condition (A17-d) on Γ yield:

$$\forall \pi \in \mathcal{P} \qquad \frac{1}{i\omega\eta}\int_\Omega \underline{\mathrm{grad}}_y(\pi).\mathbf{K}.\underline{\mathrm{grad}}_y(\widetilde{p})\,\mathrm{d}\Omega = \int_\Omega \left(\boldsymbol{\alpha} : \mathbf{e}_y(\widetilde{\underline{u}}) + \frac{\widetilde{p}}{M} + \boldsymbol{\alpha} : (\mathbf{e}_x(\underline{U}) + \mathbf{e}_y(\underline{u}_0^1)) + \frac{P_p}{M}\right)\pi\,\mathrm{d}\Omega.$$

Then, using relation (A21), we derive the following variational formulation defining $\widetilde{p}$:

$$\forall \pi \in \mathcal{P},\ \int_\Omega (\underline{\mathrm{grad}}_y(\pi).\frac{\mathbf{K}}{i\omega\eta}.\underline{\mathrm{grad}}_y(\widetilde{p}) + \frac{\pi\widetilde{p}}{M} + \mathbf{e}_y(\widetilde{\underline{u}}(\pi)) : \mathbf{c} : \mathbf{e}_y(\widetilde{\underline{u}}(\widetilde{p})))\,\mathrm{d}\Omega = -\int_\Omega \left(\boldsymbol{\alpha} : (\mathbf{e}_x(\underline{U}) + \mathbf{e}_y(\underline{u}_0^1)) + \frac{P_p}{M}\right)\pi\,\mathrm{d}\Omega. \tag{A23}$$

Owing to the symmetry and ellipticity of the left-hand side term, and to the definition of $\underline{u}_0$ given by (A9), we deduce the existence and uniqueness of $\widetilde{p}$, which can be expressed in the following form:

$$\widetilde{p}(\underline{x}, \underline{y}) = \widetilde{\boldsymbol{\theta}} : \mathbf{e}_x(\underline{U}) - \widetilde{\varpi}P_p = \widetilde{\theta}^{ij}(\underline{y})\mathrm{e}_{xij}(\underline{U}) - \widetilde{\varpi}(\underline{y})P_p. \tag{A24}$$

Then, substituting this expression in eq. (A19) allows determining $\widetilde{\underline{u}}(x, y)$ (modulo an uniform translation field) in the form:

$$\widetilde{\underline{u}}(\underline{x}, \underline{y}) = \widetilde{\boldsymbol{\xi}}(\underline{y}) : \mathbf{e}_x(\underline{U}) - \widetilde{\underline{\zeta}}(\underline{y})P_p \qquad \text{where} \qquad \widetilde{\underline{\xi}}^{ij} = \widetilde{\underline{u}}(\widetilde{\theta}^{ij}); \quad \widetilde{\underline{\zeta}} = \widetilde{\underline{u}}(\widetilde{\varpi}). \tag{A25}$$

Note that the motions $\widetilde{\underline{\xi}}^{ij}$ and $\widetilde{\underline{\zeta}}$ (of zero mean value on Ω) are complex valued and frequency dependent, just like the pressure fields $\widetilde{\theta}^{ij}$ and $\widetilde{\varpi}$. Finally, the local fields at any frequency are given, modulo a uniform translation motion, by

$$\left.\begin{aligned} \underline{u}^1 = \widetilde{\underline{u}} + \underline{u}_0^1 = (\boldsymbol{\xi}_0 + \widetilde{\boldsymbol{\xi}}(\omega)) : \mathbf{e}_x(\underline{U}) - (\underline{\zeta}_0 + \widetilde{\underline{\zeta}}(\omega))P_p \\ p^0 = \widetilde{p} + P_p = \widetilde{\boldsymbol{\theta}}(\omega) : \mathbf{e}_x(\underline{U}) + (1 - \widetilde{\varpi}(\omega))P_p \end{aligned}\right\} \tag{A26}$$

A3.4 Spectral decomposition of $\underline{\widetilde{u}}$ and $\widetilde{p}$

As in Hornung & Showalter (1990) and Auriault & Royer (1993) for rigid porous media, let us consider the eigenvalue problem associated with the pressure diffusion operator in eq. (A17-c) with condition (A17-d) on the boundary

$$\left.\begin{aligned} \mathrm{div}_y(\mathbf{K}.\underline{\mathrm{grad}}_y(\Psi)) &= -\kappa\Psi \qquad \text{in } \Omega \\ \Psi &= 0 \qquad \text{on } \Gamma \end{aligned}\right\} \tag{A27}$$

The spectrum is discrete and positive that is, $0 \le \kappa_1 \le \kappa_2 \le \kappa_3 \le \dots$ and we have $\kappa_I = O(l|\mathbf{K}|/\ell^2)$ (remind that ℓ is the characteristic size of $\widehat{\Omega}$ and Ω). Each eigenvalue κ_I (capital indices stand for the eigenvalue rank), being associated to a eigenfunction Ψ_I (Courant & Hilbert 1970). The set $\{\Psi_I\}$ constitutes an orthogonal basis on which $\widetilde{p}$ can be composed. Thus, owing to the linearity and relation (A20) we have:

$$\left.\begin{aligned} \widetilde{p}(\underline{x},\underline{y}) &= \sum_I a_I(\omega,\underline{x})\Psi_I(\underline{y}) \\ \underline{\widetilde{u}}(\underline{x},\underline{y}) = \underline{\widetilde{u}}(\widetilde{p}) &= \sum_I a_I(\omega,\underline{x})\underline{\Upsilon}_I(\underline{y}) \quad \text{where} \quad \underline{\Upsilon}_I = \underline{\widetilde{u}}(\Psi_I) \end{aligned}\right\} \tag{A28}$$

To determine the amplitudes a_I, note first that from the divergence theorem, the periodicity and the zero pressure condition on Γ, we have

$$\int_\Omega \mathrm{div}_y(\mathbf{K}.\underline{\mathrm{grad}}_y(\Psi_I)).\widetilde{p}\,\mathrm{d}\Omega = \int_\Omega \mathrm{div}_y(\mathbf{K}.\underline{\mathrm{grad}}_y(\widetilde{p})).\Psi_I\,\mathrm{d}\Omega\,.$$

This equality re-expressed with the balance equation of both fields $\widetilde{p}$ and Ψ_I reads (no summation on $_I$ on the left-hand side)

$$-\kappa_I\int_\Omega \Psi_I\widetilde{p}\,\mathrm{d}\Omega = i\omega\eta\int_\Omega\left[\boldsymbol{\alpha}:\mathbf{e}_y(\underline{\widetilde{u}}) + \frac{\widetilde{p}}{M} + \boldsymbol{\alpha}:(\mathbf{e}_x(\underline{U}) + \mathbf{e}_y(\underline{u}_0^1)) + \frac{P_p}{M}\right]\Psi_I\,\mathrm{d}\Omega$$

and, using the orthogonality of eigenfunctions and relation (A21) we deduce the linear system governing the coefficients $a_I(\omega)$ (no summation on $_I$):

$$\left.\begin{aligned} -\left[\kappa_I + i\omega\eta\left(\frac{1}{M} + D_{II}\right)\right]a_I + i\omega\eta\sum_{J\neq I} D_{IJ}a_J &= i\omega\eta\left(\mathbf{D}_I:\mathbf{e}_x(\underline{U}) + \mathcal{D}_I\frac{P_p}{M}\right) \\ D_{IJ} &= \frac{\int_\Omega \mathbf{e}_y(\underline{\Upsilon}_I):\mathbf{c}:\mathbf{e}_y(\underline{\Upsilon}_J)\,\mathrm{d}\Omega}{\int_\Omega \Psi_I^2\,\mathrm{d}\Omega} \\ \mathbf{D}_I = \boldsymbol{\alpha}\mathcal{D}_I + \frac{\int_\Omega \boldsymbol{\alpha}:\mathbf{e}_y(\boldsymbol{\xi}_0)\Psi_I\,\mathrm{d}\Omega}{\int_\Omega \Psi_I^2\,\mathrm{d}\Omega};\quad \mathcal{D}_I &= \frac{\int_\Omega \Psi_I\,\mathrm{d}\Omega}{\int_\Omega \Psi_I^2\,\mathrm{d}\Omega} \end{aligned}\right\} \tag{A29}$$

where $D_{II} = O(|\mathbf{c}|^{-1})$, $\mathbf{D}_I$ and $\mathcal{D}_I$ are frequency-independent terms.

In the full decoupling case where $D_{IJ} = D_I\delta_{IJ}$, the orthogonality of the pressure eigenmodes also applies for the associated motions. Then the amplitude of the eigenmodes are uncoupled and we have

$$a_I(\omega,\underline{x}) = -\frac{1}{\frac{\kappa_I}{i\omega\eta} + \frac{1}{M} + D_I}\left(\mathbf{D}_I:\mathbf{e}_x(\underline{U}) + \mathcal{D}_I\frac{P_p}{M}\right).$$

A3.5 Frequency dependence at low and high frequency

When $\omega \to 0$, the fields $\underline{\widetilde{u}}$ and $\widetilde{p}$ vanish by construction. More precisely the differential set (A17) shows that $\underline{\widetilde{u}}$ and $\widetilde{p}$ (hence $\widetilde{\boldsymbol{\xi}}$, $\widetilde{\boldsymbol{\theta}}$ and $\underline{\widetilde{\zeta}}$, $\widetilde{\varpi}$) are imaginary and depend linearly on the frequency, that is, $\underline{\widetilde{u}} \approx i\omega\eta\underline{\mathrm{u}}$, $\widetilde{p} \approx i\omega\eta\mathrm{p}$, where p and $\underline{\mathrm{u}}$ are real valued fields solutions to:

$$\left.\begin{aligned} \mathrm{div}_y\left(\mathbf{c}:\mathbf{e}_y(\underline{\mathrm{u}}) - \boldsymbol{\alpha}\mathrm{p}\right) &= \underline{0} \qquad \text{in } \Omega \\ \left(\mathbf{c}:\mathbf{e}_y(\underline{\mathrm{u}}) - \boldsymbol{\alpha}\mathrm{p}\right).\underline{n} &= \underline{0} \qquad \text{on } \Gamma \\ \mathrm{div}_y(\mathbf{K}.\underline{\mathrm{grad}}_y(\mathrm{p})) = \boldsymbol{\alpha}:(\mathbf{e}_x(\underline{U}) + \mathbf{e}_y(\underline{u}_0^1)) + \frac{P_p}{M} &\qquad \text{in } \Omega \\ \mathrm{p} &= 0 \qquad \text{on } \Gamma \\ \underline{\mathrm{u}} \text{ and } \mathrm{p}, \quad \widehat{\Omega} &- \text{periodic} \end{aligned}\right\} \tag{A30}$$

When $\omega \to \infty$, we have $\widetilde{\boldsymbol{\xi}} \to \boldsymbol{\xi}_\infty - \boldsymbol{\xi}_0$, $\underline{\widetilde{\zeta}} \to \zeta_\infty - \zeta_0$, $\widetilde{\boldsymbol{\theta}} \to \boldsymbol{\theta}_\infty$ and $\widetilde{\varpi} \to \varpi_\infty$. The pressure $p_\infty = -M\boldsymbol{\alpha}:\left(\mathbf{e}_x(\underline{U}) + \mathbf{e}_y(\underline{u}_\infty^1)\right)$ within Ω is determined through the mass balance (4.2–c), independently of the boundary condition $p^0 = P_p$ on Γ. This means that, at 'infinite' frequency, there is a jump of pressure on Γ. Consequently, when $\omega \to \infty$ a boundary layer of small thickness $|\delta|$ appears on Γ in order to match the

micropore pressure p_∞ and the pore pressure P_p. To determine these boundary layer fields at high frequency, it is convenient to decompose $(\underline{u}^1, p^0)$ into the sum of the short-term solution $(\underline{u}_\infty, p_\infty)$ and the frequency-dependent fields $(\underline{\breve{u}}(\omega), \breve{p}(\omega))$, that is,

$$\underline{u}^1 = \underline{u}^1_\infty + \underline{\breve{u}}(\omega); \qquad p^0 = p_\infty + \breve{p}(\omega).$$

We then deduce that $(\underline{\breve{u}}, \breve{p})$ is the solution to the following differential set of equations

$$\left.\begin{aligned}
\underline{\mathrm{div}}_y\left(\mathbf{c} : \mathbf{e}_y(\underline{\breve{u}})\right) - \boldsymbol{\alpha}\breve{p}\right) &= \underline{0} && \text{in } \Omega \\
\left(\mathbf{c} : \mathbf{e}_y(\underline{\breve{u}})\right) - \boldsymbol{\alpha}\breve{p}\right) .\underline{n} &= \underline{0} && \text{on } \Gamma \\
\frac{1}{i\omega\eta}\mathrm{div}_y(\mathbf{K}.\underline{\mathrm{grad}}_y(-M\boldsymbol{\alpha} : \mathbf{e}_y(\underline{u}^1_\infty) + \breve{p})) &= \boldsymbol{\alpha} : \mathbf{e}_y(\underline{\breve{u}}) + \frac{1}{M}\breve{p} && \text{in } \Omega \\
\breve{p} &= P_p - p_\infty && \text{on } \Gamma \\
\breve{p} \to 0; \qquad \underline{\breve{u}} &\to \underline{0} && \text{'inside' } \Omega \\
\underline{\breve{u}} \quad \text{and} \quad \breve{p}, \quad & \widehat{\Omega}-\text{periodic}
\end{aligned}\right\} \tag{A31}$$

To make the analysis clearer, we focus on the isotropic case so that the balance equations (A31-a) and (A31-c) take the following form:

$$\left.\begin{aligned}
(\lambda+\mu)\underline{\mathrm{grad}}_y(\mathrm{div}_y(\underline{\breve{u}})) + \mu\underline{\Delta}_y(\underline{\breve{u}}) - \alpha\underline{\mathrm{grad}}_y(\breve{p}) &= \underline{0} \\
\frac{\mathrm{K}}{i\omega\eta}\Delta_y(\breve{p} - M\alpha\mathrm{div}_y(\underline{u}^1_\infty)) &= \alpha\mathrm{div}_y(\underline{\breve{u}}) - \frac{1}{M}\breve{p},
\end{aligned}\right\} \tag{A32}$$

By construction $\underline{u}^1_\infty$ satisfies the balance equation, (see eq. A11-a):

$$(\lambda_\infty+\mu)\underline{\mathrm{grad}}_y(\mathrm{div}_y(\underline{u}^1_\infty)) + \mu\Delta_y(\underline{u}^1_\infty) = \underline{0},$$

and therefore:

$$(\lambda_\infty + 2\mu)\Delta_y(\mathrm{div}_y(\underline{u}^1_\infty)) = 0.$$

Consequently, the term related to $\underline{u}^1_\infty$ vanishes in eq. (A32-b). Now, boundary fields exist within a very thin layer close to the interface Γ, symbolically denoted by $|\delta| \times \Gamma$. Thus, at the scale of the boundary layer, Γ can be assimilated to its tangent plane, and fields $(\underline{\breve{u}}, \breve{p})$ essentially vary along the normal of Γ. This leads introducing the 'dilated' abscissa z_n along the normal such that $z_n = 0$ on Γ, and $z_n \to \infty$ on the inner limit of $|\delta| \times \Gamma$. The field is governed by the following set of equations, where $\breve{u}_n$, $\breve{u}_{t_1}$, $\breve{u}_{t_2}$ stand for the components of $\underline{\breve{u}}$ along the normal and along the tangent vectors of Γ:

$$\left.\begin{aligned}
(\lambda+2\mu)\breve{u}_{n,z_nz_n} - \alpha\breve{p}_{,z_n} = 0; \quad \mu\breve{u}_{t_1,z_nz_n} = \mu\breve{u}_{t_2,z_nz_n} &= 0 && \text{in } |\delta| \times \Gamma \\
(\lambda+2\mu)\breve{u}_{n,z_n} - \alpha\breve{p} = 0; \quad \mu\breve{u}_{t_1,z_n} = \mu\breve{u}_{t_2,z_n} &= 0 && \text{on } \Gamma \quad \text{that is,} \quad z_n = 0 \\
\frac{\mathrm{K}}{i\omega\eta}\breve{p}_{,z_nz_n} - \alpha\breve{u}_{n,z_n} - \frac{\breve{p}}{M} &= 0 && \text{in } |\delta| \times \Gamma \\
\breve{p} &= P_p - p_\infty && \text{on } \Gamma \quad \text{that is,} \quad z_n = 0 \\
\breve{p} \to 0; \qquad \underline{\breve{u}} &\to \underline{0} && \text{'inside' } \Omega \quad \text{that is,} \quad z_n \to \infty \\
\underline{\breve{u}} \quad \text{and} \quad \breve{p}, \quad & \widehat{\Omega}-\text{periodic}
\end{aligned}\right\} \tag{A33}$$

By simple integration and taking the boundary conditions into account we obtain that $\breve{u}_{t_1}(z_n) = \breve{u}_{t_2}(z_n) = 0$. Further, $(\lambda+2\mu)\breve{u}_{n,z_n} - \alpha\breve{p} = 0$, then, recalling that $\frac{1}{B} = \frac{1}{M} + \frac{\alpha^2}{\lambda+2\mu}$, $\breve{p}$ is defined by :

$$\frac{\mathrm{K}}{i\omega\eta}\breve{p}_{,z_nz_n} - \frac{\breve{p}}{B} = 0; \qquad \breve{p}_{|z_n=0} = P_p - p_\infty; \qquad \breve{p}_{|z_n\to\infty} \to 0$$

Consequently, introducing the frequency-dependent complex thickness $\delta = \sqrt{\frac{K_B}{i\,\omega\eta}}$, the boundary layer fields close to any point M_Γ of Γ read

$$\check{p}_{|M_\Gamma} = [P_p - p_{\infty|M_\Gamma}]\exp(-z_n/\delta) \quad \text{and} \quad \check{u}_{n|M_\Gamma} = \frac{\alpha}{\lambda+2\mu}\int_0^{z_n} \check{p}_{|M_\Gamma}\mathrm{d}z.$$

The mean value of $\check{p}$ is given by

$$\frac{1}{\widehat{\Omega}}\int_\Omega \check{p}_{|M_\Gamma}\mathrm{d}\Omega = \frac{1}{\widehat{\Omega}}\int_\Gamma \mathrm{d}\Gamma\int_0^\infty \check{p}_{|M_\Gamma}\mathrm{d}z = -\delta\left[P_p - \frac{1}{\Gamma}\int_\Gamma p_\infty \mathrm{d}\Gamma\right]\frac{\Gamma}{\widehat{\Omega}},$$

and, replacing p_∞ by its expression (A15-a), we have

$$\frac{1}{\widehat{\Omega}}\int_\Omega \check{p}\,\mathrm{d}\Omega = \frac{\delta\,\Gamma}{\widehat{\Omega}}\left[-P_p\frac{\int_\Gamma \varpi_\infty \mathrm{d}\Gamma}{\Gamma} + \mathbf{e}_x(\underline{U}) : \frac{\int_\Gamma \boldsymbol{\theta}_\infty \mathrm{d}\Gamma}{\Gamma}\right]. \tag{A34}$$

At any point M_Γ of Γ, the stress $\check{\boldsymbol{\sigma}}$ is related to $\check{p}$ by the relation:

$$\check{\boldsymbol{\sigma}}_{|M_\Gamma} = \lambda\check{u}_{n,z_n}\mathbf{I} + 2\mu\check{u}_{n,z_n}\underline{n}\otimes\underline{n} = \left(\frac{\lambda}{\lambda+2\mu}\mathbf{I} + \frac{2\mu}{\lambda+2\mu}\underline{n}\otimes\underline{n}\right)\alpha\check{p}_{|M_\Gamma}.$$

Then, the mean value is expressed as follows:

$$\begin{aligned}\frac{1}{\widehat{\Omega}}\int_\Omega \check{\boldsymbol{\sigma}}\,\mathrm{d}\Omega &= \frac{1}{\widehat{\Omega}}\int_\Gamma \alpha\left(\frac{\lambda}{\lambda+2\mu}\mathbf{I} + \frac{2\mu}{\lambda+2\mu}\underline{n}\otimes\underline{n}\right)\mathrm{d}\Gamma\int_0^\infty \check{p}_{|M_\Gamma}\mathrm{d}z \\ &= \frac{\delta\,\Gamma}{\widehat{\Omega}}\frac{\alpha}{\lambda+2\mu}\left[-P_p\frac{\int_\Gamma(\lambda\mathbf{I}+2\mu\underline{n}\otimes\underline{n})\varpi_\infty\mathrm{d}\Gamma}{\Gamma} + \mathbf{e}_x(\underline{U}) : \frac{\int_\Gamma(\lambda\mathbf{I}+2\mu\underline{n}\otimes\underline{n})\boldsymbol{\theta}_\infty\mathrm{d}\Gamma}{\Gamma}\right].\end{aligned} \tag{A35}$$

Relations (A34–A35) show that the mean value of the high-frequency boundary layer fields of pressure and stress are in phase quadrature with the forcing terms P_p and $\mathbf{e}_x(\underline{U})$ (recall that ϖ_∞ and $\boldsymbol{\theta}_\infty$ are real quantities). They depend on the dimensionless parameter $\frac{\delta\,\Gamma}{\widehat{\Omega}}$, that varies with frequency as $1/\sqrt{\omega}$, and involves the interface area between the microporous domain and the pores. In the anisotropic case, similar results will be obtained, however, the boundary layer thickness will depend on the orientation of the interface. Thus, expression (4.11) only provides an estimate (with K and B replaced by the order of magnitude of the principal values of tensor $\mathbf{K}$ and $\mathbf{c} + M\boldsymbol{\alpha}\otimes\boldsymbol{\alpha}$).

A4 Momentum balance

The macroscopic model is finally established by deriving the momentum and mass balance equations at the leading order, from the local problems in both the pore and the microporous domains at the second order.

The momentum balance in both domains lead to the following set of equations with the associated stress continuity:

$$\left.\begin{aligned} \underline{\mathrm{div}}_y(\boldsymbol{\Sigma}^1) + \underline{\mathrm{div}}_x(\boldsymbol{\Sigma}^0) &= \underline{0} && \text{in } \Omega \\ \boldsymbol{\Sigma}^1.\underline{n} = \boldsymbol{\sigma}_p^1.\underline{n} &= \left(-p_p^1\mathbf{I} + 2\eta D_y(\underline{v}_p^0)\right).\underline{n} && \text{on } \Gamma \\ \underline{\mathrm{div}}_y(\boldsymbol{\sigma}_p^{\,1}) - \underline{\mathrm{grad}}_x(P_p) &= \underline{0} && \text{in } \Omega' \\ \boldsymbol{\Sigma}^1 \quad \text{and} \quad \boldsymbol{\sigma}^1, \quad \widehat{\Omega} &- \text{periodic} \end{aligned}\right\} \tag{A36}$$

Integrating these equations over each volume, and accounting for the boundary condition and periodicity leads to the balance equation governing the macroscopic total stress tensor $\mathbf{S}^0$ of the double porosity medium:

$$\underline{\mathrm{div}}_x(\mathbf{S}) = 0; \qquad \mathbf{S} = \frac{1}{\widehat{\Omega}}\int_\Omega \boldsymbol{\Sigma}^0\,\mathrm{d}\Omega - \phi_p P_p\mathbf{I} \tag{A37}$$

Knowing that $\boldsymbol{\Sigma} = \mathbf{c} : (\mathbf{e}_x(\underline{U}) + \mathbf{e}_y(\underline{u}^1)) - \boldsymbol{\alpha}p^0$, where $\underline{u}^1$ and p^0 are given by eq. (A26), the constitutive law for the macroscopic total stress tensor reads:

$$\mathbf{S} = \mathbf{C}(\omega) : \mathbf{e}_x(\underline{U}) - \mathbf{A}(\omega)P_p. \tag{A38}$$

The effective tensors $\mathbf{C}(\omega)$ and $\mathbf{A}(\omega)$ can be decomposed into the elastic tensors $\mathbf{C}_0$ and $\mathbf{A}_0$ corresponding to the long-term elastic response and the frequency-dependent tensors $\widetilde{\mathbf{C}}(\omega)$ and $\widetilde{\mathbf{A}}(\omega)$. Their expressions are related to the local fields as follows:

$$\left.\begin{aligned}
\mathbf{C}(\omega) &= \mathbf{C}_0 + \widetilde{\mathbf{C}}(\omega)\\
\mathbf{C}_0 &= \frac{1}{\widehat{\Omega}}\int_\Omega \left(\mathbf{c} + \mathbf{c} : \mathbf{e}_y(\boldsymbol{\xi}_0)\right)\,\mathrm{d}\Omega\\
\widetilde{\mathbf{C}}(\omega) &= \frac{1}{\widehat{\Omega}}\int_\Omega \left(\mathbf{c} : \mathbf{e}_y(\widetilde{\boldsymbol{\xi}}) - \boldsymbol{\alpha}\otimes\widetilde{\boldsymbol{\theta}}\right)\,\mathrm{d}\Omega\\
\mathbf{A}(\omega) &= \mathbf{A}_0 + \widetilde{\mathbf{A}}(\omega)\\
\mathbf{A}_0 &= \phi_p\mathbf{I} + \frac{1}{\widehat{\Omega}}\int_\Omega \left(\boldsymbol{\alpha} + \mathbf{c} : \mathbf{e}_y(\underline{\zeta}_0)\right)\,\mathrm{d}\Omega\\
\widetilde{\mathbf{A}}(\omega) &= \frac{1}{\widehat{\Omega}}\int_\Omega \left(-\boldsymbol{\alpha}\widetilde{\varpi} + \mathbf{c} : \mathbf{e}_y(\underline{\widetilde{\zeta}})\right)\,\mathrm{d}\Omega
\end{aligned}\right\} \tag{A39}$$

According to the results obtained in the previous section, at low frequency we have

$$\widetilde{\mathbf{C}}(\omega) \to i\omega\eta\mathbb{C}; \qquad \widetilde{\mathbf{A}}(\omega) \to i\omega\eta\mathbb{A} \qquad \text{when} \qquad \omega \to 0 \tag{A40}$$

where $\mathbb{C}_0$ and $\mathbb{A}_0$ are dimensionless and real valued.

Similarly, $\mathbf{C}(\omega)$ and $\mathbf{A}(\omega)$ can be decomposed into the short-term tensors (high-frequency limit, purely elastic, hence real) $\mathbf{C}_\infty$ and $\mathbf{A}_\infty$ and the frequency-dependent tensors $\check{\mathbf{C}}(\omega)$ and $\check{\mathbf{A}}(\omega)$. Their expressions are given by:

$$\left.\begin{aligned}
\mathbf{C}(\omega) &= \mathbf{C}_\infty + \check{\mathbf{C}}(\omega); \qquad \mathbf{C}_\infty = \frac{1}{\widehat{\Omega}}\int_\Omega \left(\mathbf{c} + \mathbf{c} : \mathbf{e}_y(\boldsymbol{\xi}_\infty) - \boldsymbol{\alpha}\otimes\boldsymbol{\theta}_\infty\right)\,\mathrm{d}\Omega\\
\mathbf{A}(\omega) &= \mathbf{A}_\infty + \check{\mathbf{A}}(\omega); \qquad \mathbf{A}_\infty = \phi_p\mathbf{I} + \frac{1}{\widehat{\Omega}}\int_\Omega (\boldsymbol{\alpha} + \mathbf{c} : \mathbf{e}_y(\underline{\zeta}_\infty) - \boldsymbol{\alpha}\varpi_\infty)\,\mathrm{d}\Omega
\end{aligned}\right\} \tag{A41}$$

In the isotropic case, the analysis developed in the previous section provides

$$\left.\begin{aligned}
\check{\mathbf{C}}(\omega) &= \sqrt{\frac{KB}{i\omega\eta}}\frac{2\alpha\int_\Gamma((\lambda+\mu)\mathbf{I} + \mu\underline{n}\otimes\underline{n})\otimes\boldsymbol{\theta}_\infty\mathrm{d}\Gamma}{\widehat{\Omega}(\lambda+2\mu)} \qquad \text{when} \qquad \omega\to\infty\\
\check{\mathbf{A}}(\omega) &= \sqrt{\frac{KB}{i\omega\eta}}\frac{2\alpha\int_\Gamma((\lambda+\mu)\mathbf{I} + \mu\underline{n}\otimes\underline{n})\varpi_\infty\mathrm{d}\Gamma}{\widehat{\Omega}(\lambda+2\mu)} \qquad \text{when} \qquad \omega\to\infty
\end{aligned}\right\} \tag{A42}$$

Finally, using the spectral decomposition (A28), we may also write

$$\left.\begin{aligned}
\mathbf{S} &= \mathbf{C}_0 : \mathbf{e}_x(\underline{U}) - \mathbf{A}_0 P_p + \sum_I a_I(\omega)(\mathbf{s}_I - \boldsymbol{\alpha}\mathcal{P}_I)\\
\mathbf{s}_I &= \frac{1}{\widehat{\Omega}}\int_\Omega \mathbf{c} : \mathbf{e}_y(\underline{\Upsilon}_I)\,\mathrm{d}\Omega; \qquad \mathcal{P}_I = \frac{1}{\widehat{\Omega}}\int_\Omega \Psi_I\,\mathrm{d}\Omega
\end{aligned}\right\} \tag{A43}$$

where $\mathbf{s}_I$ and $\mathcal{P}_I$ stand for the mean stress and mean pressure associated to the eigenpressure Ψ_I. Note that, according to (A29-a), the coefficients a_I are defined by

$$\left(\kappa_I + \frac{i\omega\eta}{M}\right)a_I + i\omega\eta D_{IJ}a_J = -i\omega\eta\left(\mathbf{D}_I : \mathbf{e}_x(\underline{U}) + \mathcal{D}_I\frac{P_p}{M}\right). \tag{A44}$$

A5 Mass balance

For mass balance we have

$$\left.\begin{aligned}
\phi\mathrm{div}_y(\underline{v}_f^1 - i\omega\underline{u}^1) &= -i\omega\left[\boldsymbol{\alpha} : \left(\mathbf{e}_y(\underline{u}^1) + \mathbf{e}_x(\underline{U})\right) + \frac{p^0}{M}\right] \qquad \text{in } \Omega\\
\phi(\underline{v}_f^1 - i\omega\underline{u}^1).\underline{n} &= (\underline{v}_p^1 - i\omega\underline{u}^1).\underline{n} \qquad \text{on } \Gamma\\
\mathrm{div}_y(\underline{v}_p^1) + \mathrm{div}_x(\underline{v}_p^0) &= -i\omega\frac{P_p}{K_f} \qquad \text{in } \Omega_p\\
\underline{v}_f^1 \quad \underline{u}^1 \quad &\text{and} \quad \underline{v}_p^1, \quad \widehat{\Omega}-\text{periodic}
\end{aligned}\right\} \tag{A45}$$

Integrating these equations over each volume, and accounting for the boundary condition and periodicity, lead to:

$$\int_\Omega i\omega \operatorname{div}_y(\underline{u}^1)\,\mathrm{d}\Omega + \int_{\Omega_p} \operatorname{div}_x(\underline{v}_p^0)\,\mathrm{d}\Omega = -i\omega\left[|\Omega_p|\frac{P_p}{K_f} + \int_\Omega \left(\boldsymbol{\alpha} : \left(\mathbf{e}_y(\underline{u}^1) + \mathbf{e}_x(\underline{U})\right) + \frac{p^0}{M}\right)\mathrm{d}\Omega\right]$$

which is rewritten as:

$$\phi_p \operatorname{div}_x(\underline{V}_p - i\omega\underline{U}) = -i\omega\phi_p\left(\operatorname{div}_x(\underline{U}) + \frac{P_p}{K_f}\right) - i\omega\frac{1}{|\widehat{\Omega}|}\int_\Omega \left(\boldsymbol{\alpha} : (\mathbf{e}_y(\underline{u}^1) + \mathbf{e}_x(\underline{U})) - \operatorname{div}_y(\underline{u}^1) + \frac{p^0}{M}\right)\mathrm{d}\Omega$$

Replacing the local fields $(\underline{u}^1, p^0)$ by their expressions (A26), the macroscopic mass balance governing the double porosity medium takes the form:

$$\phi \operatorname{div}_x(\underline{V}_p - i\omega\underline{U}) = -i\omega\left(\mathbf{B}(\omega) : \mathbf{e}_x(\underline{U}) + \frac{P_p}{\mathcal{M}(\omega)}\right). \tag{A46}$$

The effective tensor $\mathbf{B}$ and scalar $\mathcal{M}^{-1}$ are respectively the sum of the tensor $\mathbf{B}_0$ and scalar $\mathcal{M}_0^{-1}$—corresponding to the long-term response—and the frequency-dependent tensor $\widetilde{\mathbf{B}}(\omega)$ and scalar $\widetilde{\mathcal{M}}^{-1}(\omega)$. Their expressions are related to the local fields as follows:

$$\left.\begin{aligned}
\mathbf{B}(\omega) &= \mathbf{B}_0 + \widetilde{\mathbf{B}}(\omega)\\
\mathbf{B}_0 &= \phi_p\mathbf{I} + \frac{1}{\widehat{\Omega}}\int_\Omega (\boldsymbol{\alpha} + \boldsymbol{\alpha} : \mathbf{e}_y(\boldsymbol{\xi}_0) - \operatorname{div}_y(\boldsymbol{\xi}_0))\,\mathrm{d}\Omega\\
\widetilde{\mathbf{B}}(\omega) &= \frac{1}{\widehat{\Omega}}\int_\Omega \left(\boldsymbol{\alpha} : \mathbf{e}_y(\widetilde{\boldsymbol{\xi}}) - \operatorname{div}_y(\widetilde{\boldsymbol{\xi}}) + \frac{\widetilde{\theta}}{M}\right)\mathrm{d}\Omega\\
\frac{1}{\mathcal{M}(\omega)} &= \frac{1}{\mathcal{M}_0} + \frac{1}{\widetilde{\mathcal{M}}(\omega)}\\
\frac{1}{\mathcal{M}_0} &= \frac{\phi_p}{K_f} + \frac{1-\phi_p}{M} - \frac{1}{\widehat{\Omega}}\int_\Omega (\boldsymbol{\alpha} : \mathbf{e}_y(\underline{\zeta}_0) - \operatorname{div}_y(\underline{\zeta}_0))\,\mathrm{d}\Omega\\
\frac{1}{\widetilde{\mathcal{M}}(\omega)} &= -\frac{1}{\widehat{\Omega}}\int_\Omega \left(\boldsymbol{\alpha} : \mathbf{e}_y(\widetilde{\underline{\zeta}}) - \operatorname{div}_y(\widetilde{\underline{\zeta}}) + \frac{\widetilde{\varpi}}{M}\right)\mathrm{d}\Omega
\end{aligned}\right\} \tag{A47}$$

From the results obtained in the previous section, at low frequency we have:

$$\widetilde{\mathbf{B}}(\omega) \to \frac{i\omega\eta}{M}\mathbb{B}; \qquad \frac{1}{\widetilde{\mathcal{M}}} \to \frac{i\omega\eta}{M}\frac{\mathbb{M}^{-1}}{M} \qquad \text{when} \qquad \omega \to 0 \tag{A48}$$

where $\mathbb{B}$ and $\mathbb{M}$ are dimensionless, real valued, and $O(\mathbb{B}) = O(\mathbb{M}^{-1}) = O(\Gamma/|\mathbf{K}|)$.

The high-frequency limit $\mathbf{B}_\infty$ and $\mathcal{M}_\infty^{-1}$ of $\mathbf{B}$ and $\mathcal{M}^{-1}$, are purely elastic, thus real, and read

$$\left.\begin{aligned}
\mathbf{B}_\infty &= \phi_p\mathbf{I} + \frac{1}{\widehat{\Omega}}\int_\Omega \left(\boldsymbol{\alpha} + \boldsymbol{\alpha} : \mathbf{e}_y(\boldsymbol{\xi}_\infty) - \operatorname{div}_y(\boldsymbol{\xi}_\infty) + \frac{\boldsymbol{\theta}_\infty}{M}\right)\mathrm{d}\Omega\\
\frac{1}{\mathcal{M}_\infty} &= \frac{\phi_p}{K_f} - \frac{1-\phi_p}{M} - \frac{1}{\widehat{\Omega}}\int_\Omega \left(\boldsymbol{\alpha} : \mathbf{e}_y(\underline{\zeta}_\infty) - \operatorname{div}_y(\underline{\zeta}_\infty) + \frac{\varpi_\infty}{M}\right)\mathrm{d}\Omega
\end{aligned}\right\} \tag{A49}$$

We can also decompose $\mathbf{B}$ and $\mathcal{M}^{-1}$ into short-terms and frequency-dependent terms $\check{\mathbf{B}}$ and $\check{\mathcal{M}}^{-1}$, that is,

$$\mathbf{B}(\omega) = \mathbf{B}_\infty + \check{\mathbf{B}}(\omega); \qquad \mathcal{M}^{-1}(\omega) = \mathcal{M}_\infty^{-1} + \check{\mathcal{M}}^{-1}(\omega) \tag{A50}$$

From the analysis developed in the previous section, in the isotropic case we have

$$\left.\begin{aligned}
\check{\mathbf{B}}(\omega) &= \sqrt{\frac{KB}{i\omega\eta}}\left(\frac{\alpha(\alpha-1)}{\lambda+2\mu} + \frac{1}{M}\right)\frac{\int_\Gamma \boldsymbol{\theta}_\infty\,\mathrm{d}\Gamma}{\widehat{\Omega}} \qquad \text{when} \qquad \omega \to \infty\\
\check{\mathcal{M}}^{-1}(\omega) &= \sqrt{\frac{KB}{i\omega\eta}}\left(\frac{\alpha(\alpha-1)}{\lambda+2\mu} + \frac{1}{M}\right)\frac{\int_\Gamma \varpi_\infty\,\mathrm{d}\Gamma}{\widehat{\Omega}} \qquad \text{when} \qquad \omega \to \infty
\end{aligned}\right\} \tag{A51}$$

Finally, using spectral decomposition (A28) we can also write

$$\left.\begin{aligned}
\phi \operatorname{div}_x(\underline{V}_p - i\omega\underline{U}) &= -i\omega\left(\mathbf{B}_0 : \mathbf{e}_x(\underline{U}) + \frac{P_p}{M_0} + \sum_I a_I(\omega)\left(\mathcal{B}_I + \frac{\mathcal{P}_I}{M}\right)\right)\\
\mathcal{B}_I &= \frac{1}{\widehat{\Omega}}\int_\Omega [\boldsymbol{\alpha} : \mathbf{e}_y(\underline{\Upsilon}_I) - \operatorname{div}_y(\underline{\Upsilon}_I)]\,\mathrm{d}\Omega
\end{aligned}\right\} \tag{A52}$$

where the a_I and $\mathcal{P}_I$ are defined through (A29-a) and (A43-a), respectively.

A6 Extension to dynamics

In dynamics, the local description is given by the set of equations (8.1), (8.2) together with boundary conditions (3.3), and rescaled equations (3.8), (3.9). The homogenization process is almost unchanged compared to the quasi-static case. The leading order problems in Ω and Ω_p provide, as previously (*cf.* eqs (A2) and (A3)), $\underline{u}^0(\underline{x},\underline{y}) = \underline{U}(\underline{x})$, $p_p^0(\underline{x},\underline{y}) = P_p(\underline{x})$. Now, the local problem in the pores Ω_p involves an inertial term and becomes

$$\left.\begin{aligned} -\underline{\mathrm{grad}}_y(p_p^1) - \underline{\mathrm{grad}}_x(P_p) + \eta\underline{\Delta}_y(\underline{v}_p^0) &= i\omega\rho_f\underline{v}_p^0 \quad \text{in } \Omega_p \\ \mathrm{div}(\underline{v}_p^0) &= 0 \quad \text{in } \Omega_p \\ \underline{v}_p^0 - i\omega\underline{U} &= 0 \quad \text{on } \Gamma \end{aligned}\right\} \tag{A53}$$

This is the classical problem defining the dynamic Darcy's law (Auriault 1980) from which we deduce the macroscopic constitutive law (8.3)–d. The complex dynamic permeability of the pore network, $\mathcal{K}_p(\omega)$, is the mean of the particular flow fields corresponding to $\mathrm{grad}_{xj}(P_p) = \delta_{ij}$. The local problem in the microporous domain Ω is formally identical to (4.2) but the real intrinsic permeability K is replaced by the complex dynamic permeability $\mathcal{K}(\omega)$. Hence, the local fields take a similar form as eq. (A26), except that the transient particular fields, $\widetilde{\underline{\xi}}(\underline{y},\omega)$, $\widetilde{\underline{\zeta}}(\underline{y},\omega)$, $\widetilde{\underline{\theta}}(\underline{y},\omega)$ and $\widetilde{\varpi}(\underline{y},\omega)$, have to be replaced by their homologous field $\widetilde{\underline{\xi}}_{\mathcal{K}}(\underline{y},\omega)$, $\widetilde{\underline{\zeta}}_{\mathcal{K}}(\underline{y},\omega)$, $\widetilde{\underline{\theta}}_{\mathcal{K}}(\underline{y},\omega)$ and $\widetilde{\varpi}_{\mathcal{K}}(\underline{y},\omega)$ calculated with $\mathcal{K}(\omega)$ instead of K. Then, the momentum balance is derived from the following boundary-value problem:

$$\left.\begin{aligned} \underline{\mathrm{div}}_y(\boldsymbol{\Sigma}^1) + \underline{\mathrm{div}}_x(\boldsymbol{\Sigma}^0) &= -\omega^2(1-\phi)\rho_s\underline{U} + i\omega\phi\rho_f\underline{v}_f^0 \quad \text{in } \Omega \\ \boldsymbol{\Sigma}^1.\underline{n} &= \boldsymbol{\sigma}_p^1.\underline{n} \quad \text{on } \Gamma \\ \underline{\mathrm{div}}_y(\boldsymbol{\sigma}_p^1) - \underline{\mathrm{grad}}_x(P_p) &= i\omega\rho_f\underline{v}_p^0 \quad \text{in } \Omega' \\ \boldsymbol{\Sigma}^1 \quad \text{and} \quad \boldsymbol{\sigma}^1, \quad \widehat{\Omega} &- \text{periodic} \end{aligned}\right\} \tag{A54}$$

By integrating over the both volumes, we obtain the macroscopic dynamic momentum balance (8.3–a) and constitutive law (8.3–b) of the double porosity medium. Finally, the macroscopic mass balance (8.3–c) is deduced exactly as in Appendix A5. Note that the symmetry of the description (8.3) can be established exactly in the same way as in the quasi-static case developed in Appendix B.

The effective tensors $\mathbb{C}(\omega,\mathcal{K})$, $\mathbb{A}(\omega,\mathcal{K})$ and $\mathbb{M}^{-1}(\omega,\mathcal{K})$ involved in the dynamic description (8.3) can be decomposed into elastic tensors $\mathbf{C}_0$, $\mathbf{A}_0$, $\mathbb{M}_0^{-1}(\omega,\mathcal{K})$ (corresponding to the long-term elastic response) and frequency-dependent tensors $\widetilde{\mathbf{C}}_{\mathcal{K}}(\omega)$ and $\widetilde{\mathbf{A}}_{\mathcal{K}}(\omega)$, that is,

$$\mathbb{C}(\omega,\mathcal{K}) = \mathbf{C}_0 + \widetilde{\mathbf{C}}_{\mathcal{K}}(\omega)\,; \quad \mathbb{A}(\omega,\mathcal{K}) = \mathbf{A}_0 + \widetilde{\mathbf{A}}_{\mathcal{K}}(\omega)\,; \quad \mathbb{M}^{-1}(\omega,\mathcal{K}) = \mathcal{M}_0^{-1} + \widetilde{\mathcal{M}}_{\mathcal{K}}^{-1}(\omega) \tag{A55}$$

where

$$\left.\begin{aligned} \widetilde{\mathbf{C}}_{\mathcal{K}}(\omega) &= \frac{1}{\widehat{\Omega}}\int_\Omega \left(\mathbf{c} : \mathbf{e}_y(\widetilde{\underline{\xi}}_{\mathcal{K}}) - \boldsymbol{\alpha}\otimes\widetilde{\underline{\theta}}_{\mathcal{K}}\right)\mathrm{d}\Omega \\ \widetilde{\mathbf{A}}_{\mathcal{K}}(\omega) &= \frac{1}{\widehat{\Omega}}\int_\Omega \left(-\boldsymbol{\alpha}\widetilde{\varpi}_{\mathcal{K}} + \mathbf{c} : \mathbf{e}_y(\widetilde{\underline{\zeta}}_{\mathcal{K}})\right)\mathrm{d}\Omega \\ \widetilde{\mathcal{M}}_{\mathcal{K}}^{-1}(\omega) &= -\frac{1}{\widehat{\Omega}}\int_\Omega \left(\boldsymbol{\alpha} : \mathbf{e}_y(\widetilde{\underline{\zeta}}_{\mathcal{K}}) - \mathrm{div}_y(\widetilde{\underline{\zeta}}_{\mathcal{K}}) + \frac{\widetilde{\varpi}}{M}\right)\mathrm{d}\Omega \end{aligned}\right\} \tag{A56}$$

APPENDIX B: SYMMETRY PROPERTIES

In this appendix, we establish the minor and major symmetry properties of the effective tensors $\mathbf{C}(\omega)$, $\mathbf{A}(\omega)$ and $\mathbf{B}(\omega)$, and the equality $\mathbf{A}(\omega) = \mathbf{B}(\omega)$, starting from the variational formulations.

B1 Symmetry of $\mathbf{C}_0$, $\mathbf{A}_0$ and $\mathbf{B}_0$

The components of $\mathbf{C}_0$ are defined by

$$C_{0\,ijkl} = \frac{1}{\widehat{\Omega}}\int_\Omega \left(c_{ijkl} + c_{ijpq}e_{y\,pq}(\underline{\xi}_0^{kl})\right)\mathrm{d}\Omega$$

The minor symmetry $C_{0\,ijkl} = C_{0\,jikl} = C_{0\,ijlk}$ results from the minor symmetry of $\mathbf{c}$ and the definition of $\underline{\xi}_0^{kl} = \underline{\xi}_0^{lk}$. As for the major symmetry $C_{0ijkl} = C_{0klij}$, it is sufficient to establish that:

$$\frac{1}{\widehat{\Omega}}\int_\Omega c_{ijpq}e_{y\,pq}(\underline{\xi}_0^{kl})\,\mathrm{d}\Omega = \frac{1}{\widehat{\Omega}}\int_\Omega c_{klpq}e_{y\,pq}(\underline{\xi}_0^{ij})\,\mathrm{d}\Omega$$

For this purpose, consider the variational formulation (A8) taking first $\underline{u}_0 = \underline{\xi}_0^{ij}$ and $\underline{w} = \underline{\xi}_0^{kl}$ and then $\underline{u}_0 = \underline{\xi}_0^{kl}$ and $\underline{w} = \underline{\xi}_0^{ij}$. We successively obtain:

$$\int_\Omega \mathbf{e}_y(\underline{\xi}_0^{kl}) : \mathbf{c} : \mathbf{e}_y(\underline{\xi}_0^{ij})\,\mathrm{d}\Omega = -\int_\Omega e_{y\,pq}(\underline{\xi}_0^{kl}) c_{pqij}\,\mathrm{d}\Omega$$

$$\int_\Omega \mathbf{e}_y(\underline{\xi}_0^{ij}) : \mathbf{c} : \mathbf{e}_y(\underline{\xi}_0^{kl})\,\mathrm{d}\Omega = -\int_\Omega e_{y\,pq}(\underline{\xi}_0^{ij}) c_{pqkl}\,\mathrm{d}\Omega$$

Both left-hand side terms are identical. Therefore, using the major symmetry of $\mathbf{c}$, we prove the required equality that demonstrates the major symetry of $\mathbf{C}_0$.

The components of $\mathbf{A}_0$ read

$$A_{0ij} = \phi_p \delta_{ij} + \frac{1}{\overline{\Omega}} \int_\Omega \left(\alpha_{ij} + c_{ijpq} : e_{y\,pq}(\underline{\zeta}_0) \right) \mathrm{d}\Omega$$

and the symmetry is directly inherited from the symmetry of $\mathbf{c}$ and $\boldsymbol{\alpha}$.

Similarly, the symmetry of $\mathbf{B}_0$ can be seen from the expression of its components

$$B_{0ij} = \phi_p \delta_{ij} + \frac{1}{\overline{\Omega}} \int_\Omega (\alpha_{ij} + \alpha_{pq} e_{y\,pq}(\underline{\xi}_0^{ij}) - \underline{\mathrm{div}}_y(\underline{\xi}_0^{ij}))\,\mathrm{d}\Omega$$

B2 Equality $\mathbf{A}_0 = \mathbf{B}_0$

Considering the expressions of their components, to prove the equality $\mathbf{A}_0 = \mathbf{B}_0$ it is sufficient to demonstrate that:

$$\frac{1}{\overline{\Omega}} \int_\Omega c_{ijpq} e_{y\,pq}(\underline{\zeta}_0)\,\mathrm{d}\Omega = \frac{1}{\overline{\Omega}} \int_\Omega (\alpha_{pq} e_{y\,pq}(\underline{\xi}_0^{ij}) - \mathrm{div}_y(\underline{\xi}_0^{ij}))\,\mathrm{d}\Omega$$

For this purpose, consider again the variational formulation (A8), but taking first $\underline{u}_0 = \underline{\xi}_0^{ij}$ and $\underline{w} = \underline{\zeta}_0$ and then $\underline{u}_0 = \underline{\zeta}_0$ and $\underline{w} = \underline{\xi}_0^{ij}$. We successively obtain:

$$\int_\Omega \mathbf{e}_y(\underline{\zeta}_0) : \mathbf{c} : \mathbf{e}_y(\underline{\xi}_0^{ij})\,\mathrm{d}\Omega = -\int_\Omega e_{y\,pq}(\underline{\zeta}_0) c_{pqij}\,\mathrm{d}\Omega$$

$$\int_\Omega \mathbf{e}_y(\underline{\xi}_0^{ij}) : \mathbf{c} : \mathbf{e}_y(\underline{\zeta}_0)\,\mathrm{d}\Omega = \int_\Omega \mathbf{e}_y(\underline{\xi}_0^{ij}) : (\mathbf{I} - \boldsymbol{\alpha})\,\mathrm{d}\Omega = \int_\Omega (\mathrm{div}_y(\underline{\xi}_0^{ij}) - e_{y\,pq}(\underline{\xi}_0^{ij}) \alpha_{pq})\,\mathrm{d}\Omega$$

The left-hand side terms are identical in both relations, and with the symmetry of $\mathbf{c}$ we obtain the required equality that demonstrates that $\mathbf{A}_0 = \mathbf{B}_0$.

B3 Symmetry of C(ω), A(ω) and B(ω)

With the previous results, it is sufficient to demonstrate the symetry of $\widetilde{\mathbf{C}}(\omega)$, $\widetilde{\mathbf{A}}(\omega)$ and $\widetilde{\mathbf{B}}(\omega)$ only. The components of $\widetilde{\mathbf{C}}(\omega)$ are given by:

$$\widetilde{C}_{ijkl} = \frac{1}{\overline{\Omega}} \int_\Omega \left(c_{ijpq} e_{y\,pq}(\underline{\widetilde{\xi}}^{kl}) - \alpha_{ij} \widetilde{\theta}^{kl} \right) \mathrm{d}\Omega$$

The minor symmetry results from the symmetry of $\mathbf{c}$ and $\boldsymbol{\alpha}$, and from the definition of $\underline{\widetilde{\xi}}^{kl} = \underline{\widetilde{\xi}}^{lk}$. For the major symmetry, that is, $\widetilde{C}_{ijkl} = \widetilde{C}_{klij}$, we have to establish that:

$$\int_\Omega \left(c_{ijpq} e_{y\,pq}(\underline{\widetilde{\xi}}^{kl}) - \alpha_{ij} \widetilde{\theta}^{kl} \right) \mathrm{d}\Omega = \int_\Omega \left(c_{klpq} e_{y\,pq}(\underline{\widetilde{\xi}}^{ij}) - \alpha_{kl} \widetilde{\theta}^{ij} \right) \mathrm{d}\Omega$$

This is proved using the three variational formulations (A8), (A21) and (A23). Let's take $\underline{u}_0 = \underline{\xi}_0^{kl}$ and $\underline{w} = \underline{\widetilde{\xi}}^{ij}$ in the variational formulation (A8) and $\widetilde{p} = \widetilde{\theta}^{ij}$ in the variational formulation (A21) hence $\underline{\widetilde{u}}(\widetilde{p}) = \underline{\widetilde{\xi}}^{ij}$, and $\underline{\widetilde{u}}(\pi) = \underline{\xi}_0^{kl}$; we obtain the two equalities:

$$\int_\Omega \mathbf{e}_y(\underline{\widetilde{\xi}}^{ij}) : \mathbf{c} : \mathbf{e}_y(\underline{\xi}_0^{kl})\,\mathrm{d}\Omega = -\int_\Omega e_{y\,pq}(\underline{\widetilde{\xi}}^{ij}) c_{pqkl}\,\mathrm{d}\Omega$$

$$\int_\Omega \mathbf{e}_y(\underline{\xi}_0^{kl}) : \mathbf{c} : \mathbf{e}_y(\underline{\widetilde{\xi}}^{ij})\,\mathrm{d}\Omega = \int_\Omega \alpha_{pq} e_{y\,pq}(\underline{\xi}_0^{kl}) \widetilde{\theta}^{ij}\,\mathrm{d}\Omega$$

The two left-hand side terms are identical, we therefore deduce, with the symmetry of $\mathbf{c}$, that:

$$-\int_\Omega c_{klpq} e_{y\,pq}(\underline{\widetilde{\xi}}^{ij})\,\mathrm{d}\Omega = \int_\Omega \alpha_{pq} e_{y\,pq}(\underline{\xi}_0^{kl}) \widetilde{\theta}^{ij}\,\mathrm{d}\Omega$$

so it remains to prove that:

$$\int_\Omega \left(\alpha_{pq} e_{y\,pq}(\underline{\xi}_0^{ij})\widetilde{\theta}^{kl} + \alpha_{ij}\widetilde{\theta}^{kl}\right) \mathrm{d}\Omega = \int_\Omega \left(\alpha_{pq} e_{y\,pq}(\underline{\xi}_0^{kl})\widetilde{\theta}^{ij} + \alpha_{kl}\widetilde{\theta}^{ij}\right) \mathrm{d}\Omega$$

which is precisely what it is obtained from the symmetry of the variational formulation (A23) when first taking $\pi = \widetilde{\theta}^{kl}$ and $\widetilde{p} = \widetilde{\theta}^{ij}$ (hence $e_{x\,pq}(\underline{U}) = (\delta_{ip}\delta_{jq} + \delta_{jp}\delta_{iq})/2$, $\underline{u}_0^1 = \underline{\xi}_0^{ij}$, $P_p = 0$); and second considering that $\pi = \widetilde{\theta}^{ij}$ and $\widetilde{p} = \widetilde{\theta}^{kl}$ (hence $e_{x\,pq}(\underline{U}) = (\delta_{kp}\delta_{lq} + \delta_{lp}\delta_{kq})/2$, $\underline{u}_0^1 = \underline{\xi}_0^{kl}$, $P_p = 0$). Consequently, the tensors $\widetilde{\mathbf{C}}(\omega)$, and then $\mathbf{C}(\omega)$, satisfy the major symmetry: $C_{ijkl}(\omega) = C_{klij}(\omega)$.

The components of $\widetilde{\mathbf{A}}$ and $\widetilde{\mathbf{B}}$ read respectively

$$\widetilde{A}_{ij} = \frac{1}{\overline{\Omega}} \int_\Omega \left(-\alpha_{ij}\widetilde{\varpi} + c_{ijpq} e_{y\,pq}(\widetilde{\underline{\zeta}})\right) \mathrm{d}\Omega; \quad \widetilde{B}_{ij} = \frac{1}{\overline{\Omega}} \int_\Omega \left(\alpha_{pq} e_{y\,pq}(\widetilde{\underline{\xi}}^{ij}) - \mathrm{div}_y(\widetilde{\underline{\xi}}^{ij}) + \frac{\widetilde{\theta}^{ij}}{M}\right) \mathrm{d}\Omega$$

and their symmetry comes from that of $\mathbf{c}$ and $\boldsymbol{\alpha}$.

B4 Equality $\mathbf{A}(\omega) = \mathbf{B}(\omega)$

It is sufficient to establish that $\widetilde{\mathbf{A}}(\omega) = \widetilde{\mathbf{B}}(\omega)$, which will be done using the three variational formulations (A8), (A21) and (A23). In the variational formulation (A23), we first choose $\pi = \widetilde{\varpi}$ and $\widetilde{p} = \widetilde{\theta}^{ij}$ (hence $e_{x\,pq}(\underline{U}) = (\delta_{ip}\delta_{jq} + \delta_{jp}\delta_{iq})/2$, $\underline{u}_0^1 = \underline{\xi}_0^{ij}$, $P_p = 0$); and second $\pi = \widetilde{\theta}^{ij}$ and $\widetilde{p} = \widetilde{\varpi}$ (hence $P_p = 1$, $\underline{u}_0^1 = \underline{\zeta}$, $e_{x\,pq}(\underline{U}) = 0$). Because of the $(\widetilde{p}, \widetilde{\varpi})$ symmetry, we get:

$$\frac{1}{\overline{\Omega}} \int_\Omega \left(\alpha_{ij} + \alpha_{pq} e_{y\,pq}(\underline{\xi}_0^{ij})\right) \widetilde{\varpi}\, \mathrm{d}\Omega = \frac{1}{\overline{\Omega}} \int_\Omega \left(\alpha_{pq} e_{y\,pq}(\underline{\zeta}_0) - \frac{1}{M}\right) \widetilde{\theta}^{ij}\, \mathrm{d}\Omega$$

Thus,

$$\widetilde{A}_{ij} - \widetilde{B}_{ij} = -\frac{1}{\overline{\Omega}} \int_\Omega [\alpha_{pq} e_{y\,pq}(\underline{\zeta}_0)\widetilde{\theta}^{ij} + \alpha_{pq} e_{y\,pq}(\widetilde{\underline{\xi}}^{ij}) - \mathrm{div}_y(\widetilde{\underline{\xi}}^{ij})]\, \mathrm{d}\Omega$$

$$+ \frac{1}{\overline{\Omega}} \int_\Omega [c_{ijpq} e_{y\,pq}(\widetilde{\underline{\zeta}}) + \alpha_{pq} e_{y\,pq}(\underline{\xi}_0^{ij})\widetilde{\varpi}]\, \mathrm{d}\Omega$$

Now, we take $\underline{u}_0 = \underline{\zeta}_0$ and $\underline{w} = \widetilde{\underline{\xi}}^{ij}$ the variational formulation (A8) and $\widetilde{p} = \widetilde{\theta}^{ij}$, hence $\widetilde{\underline{u}}(\widetilde{p}) = \widetilde{\underline{\xi}}^{ij}$, and $\widetilde{\underline{u}}(\pi) = \underline{\zeta}_0$ in variational formulation (A21). We thus obtain the two equalities:

$$\int_\Omega \mathbf{e}_y(\widetilde{\underline{\xi}}^{ij}) : \mathbf{c} : \mathbf{e}_y(\underline{\zeta}_0)\, \mathrm{d}\Omega = \int_\Omega \mathbf{e}_y(\widetilde{\underline{\xi}}^{ij}) : (\mathbf{I} - \boldsymbol{\alpha})\, \mathrm{d}\Omega = \int_\Omega (\mathrm{div}_y(\widetilde{\underline{\xi}}^{ij}) - \alpha_{pq} e_{y\,pq}(\widetilde{\underline{\xi}}^{ij}))\, \mathrm{d}\Omega$$

$$\int_\Omega \mathbf{e}_y(\underline{\zeta}_0) : \mathbf{c} : \mathbf{e}_y(\widetilde{\underline{\xi}}^{ij})\, \mathrm{d}\Omega = \int_\Omega \alpha_{pq} e_{y\,pq}(\underline{\zeta}_0)\widetilde{\theta}^{ij}\, \mathrm{d}\Omega\,.$$

The two left-hand side terms are equals, then

$$\int_\Omega [\alpha_{pq} e_{y\,pq}(\underline{\zeta}_0)\widetilde{\theta}^{ij} + \alpha_{pq} e_{y\,pq}(\widetilde{\underline{\xi}}^{ij}) - \mathrm{div}_y(\widetilde{\underline{\xi}}^{ij})]\, \mathrm{d}\Omega = 0$$

Similarly, let's take $\underline{u}_0 = \underline{\xi}_0^{ij}$ and $\underline{w} = \widetilde{\underline{\zeta}}$ in the variational formulation (A8) and $\widetilde{p} = \widetilde{\varpi}$ in the variational formulation (A21) and considering that $\widetilde{\underline{u}}(\widetilde{p}) = \widetilde{\underline{\zeta}}$, and $\widetilde{\underline{u}}(\pi) = \underline{\xi}_0^{ij}$, we get:

$$\int_\Omega \mathbf{e}_y(\widetilde{\underline{\zeta}}) : \mathbf{c} : \mathbf{e}_y(\underline{\xi}_0^{ij})\, \mathrm{d}\Omega = -\int_\Omega e_{y\,pq}(\widetilde{\underline{\zeta}}) c_{pqij}\, \mathrm{d}\Omega$$

$$\int_\Omega \mathbf{e}_y(\underline{\xi}_0^{ij}) : \mathbf{c} : \mathbf{e}_y(\widetilde{\underline{\zeta}})\, \mathrm{d}\Omega = \int_\Omega \alpha_{pq} e_{y\,pq}(\underline{\xi}_0^{ij})\widetilde{\varpi}\, \mathrm{d}\Omega$$

and therefore

$$\int_\Omega [c_{ijpq} e_{y\,pq}(\widetilde{\underline{\zeta}}) + \alpha_{pq} e_{y\,pq}(\underline{\xi}_0^{ij})\widetilde{\varpi}]\, \mathrm{d}\Omega = 0.$$

These two results lead to $\widetilde{A}_{ij} - \widetilde{B}_{ij} = 0$ and consequently to the equality of the coupling tensors

$\mathbf{A}(\omega) = \mathbf{B}(\omega)$.